Precambrian Research 395 (2023) 107133

Contents lists available at ScienceDirect

Precambrian Research

journal homepage: www.elsevier.com/locate/precamres

From arc accretion to within-plate extension: Geochronology and geochemistry of the Neoproterozoic magmatism on the northern margin of the Yangtze Block

Yu Huang, Xiao-Lei Wang *, Jun-Yong Li, Ru-Cao Li, De-Hong Du, Chang-Hong Jiang, Lin-Sen Li, Ning Ding

State Key Laboratory for Mineral Deposits Research, School of Earth Sciences and Engineering, Nanjing University, Nanjing 210023, China

ARTICLE INFO

Keywords:
Dahongshan area
Yangtze Block
Early Neoproterozoic
A-type rocks
Tectonic transition

ABSTRACT

Early Neoproterozoic arc magmatism and arc accretion processes are fundamental issues in reconstructing the Rodinia supercontinent. In this study we present new data of zircon U-Pb geochronology, Hf-O isotopes and whole-rock geochemistry for the magmatic rocks (including 12 felsic volcanic rocks, 3 granodioritic intrusions, 8 basaltic extrusive rocks and 12 gabbroic intrusions), which are spatially independent, in the Dahongshan area on the northern margin of the Yangtze Block. The investigated intermediate-felsic rocks are dated at ca. 970 Ma, ca. 885–865 Ma, ca. 840–830 Ma and ca. 810–790 Ma by in situ ion probe and laser zircon U-Pb dating methods. The mafic rocks are dated at ca. 870 Ma by in situ ion probe. Combined with previous age data, our new geochronology results suggest continuous magmatic activities from ca. 970 Ma to ca. 790 Ma in the Dahongshan area with a magmatic flare-up at ca. 840 Ma. The ca. 970–840 Ma mafic rocks, as well as the contemporaneous intermediate-felsic rocks, show enrichments in large ion lithophile elements (LILEs) and light rare earth elements (LREEs) and depletions in high-field strength elements (HFSEs), representing arc-related tectonic settings. Zircon grains from these rocks generally have positive $\varepsilon_{Hf}(t)$ values from +7.3 to +14.7 and slightly elevated $\delta^{18}O$ values from +5.59 to +6.89, indicating a dominant juvenile source with minor supracrustal incorporation. In contrast, the ca. 830–790 Ma mafic rocks are characterized by E-MORB- (enriched mid-ocean ridge basalt) and OIB- (oceanic island basalt) like and the contemporaneous felsic rocks show characteristics of A_2-type granites, implying a within-plate extension environment. Zircon grains from the ca. 830–790 Ma felsic rocks display broad $\varepsilon_{Hf}(t)$ values from −5.7 to +15.3 and low mantle $\delta^{18}O$ values from +3.81 to +6.11, implying multiple magma sources for their generation and the imprinting of high-temperature hydrothermal alteration. The relative contributions of the mature crustal component in the Dahongshan magmas decreases from 10–20 % in the ca. 970–840 Ma felsic rocks to 0–10 % in the ca. 830–790 Ma felsic rocks. The Neoproterozoic magmatic activity on the northern margin of the Yangtze Block recorded an integrated evolution from accretion of previous oceanic arc (ca. 970–870 Ma) at ca. 870–840 Ma to within-plate extension (ca. 830–790 Ma) in response to the convergence and divergence of the supercontinent Rodinia.

1. Introduction

The supercontinent cycle plays a key role in how the Earth's interior and surface operate, interact and evolve with each other. This global tectonic motion bears significant impact on the mechanism of global plate displacement, periphery growth of continental nuclei, recycling of continental crust and surface-deep Earth material exchange (Reddy and Evans, 2009; Condie and Aster, 2010; Roberts, 2012, 2013; Hawkesworth et al., 2017, 2020; Zerkle, 2018). The rock records left behind provide insights into the early geological evolution of the Earth. Previous studies have demonstrated that ancient blocks from different locations drifted and amalgamated to form a supercontinent at certain times (Evans, 2013; Nance et al., 2014; Wang et al., 2020; Mitchell et al., 2021), which have been identified by comparisons of orogenic belts, paleomagnetism, age peaks of detrital zircon and the mafic dyke swarms (Zhao et al., 2002, 2004; Hou et al., 2008; Hawkesworth et al., 2010; Liu

* Corresponding author.
E-mail address: wxl@nju.edu.cn (X.-L. Wang).

https://doi.org/10.1016/j.precamres.2023.107133
Received 7 March 2023; Received in revised form 7 May 2023; Accepted 4 July 2023
Available online 22 July 2023

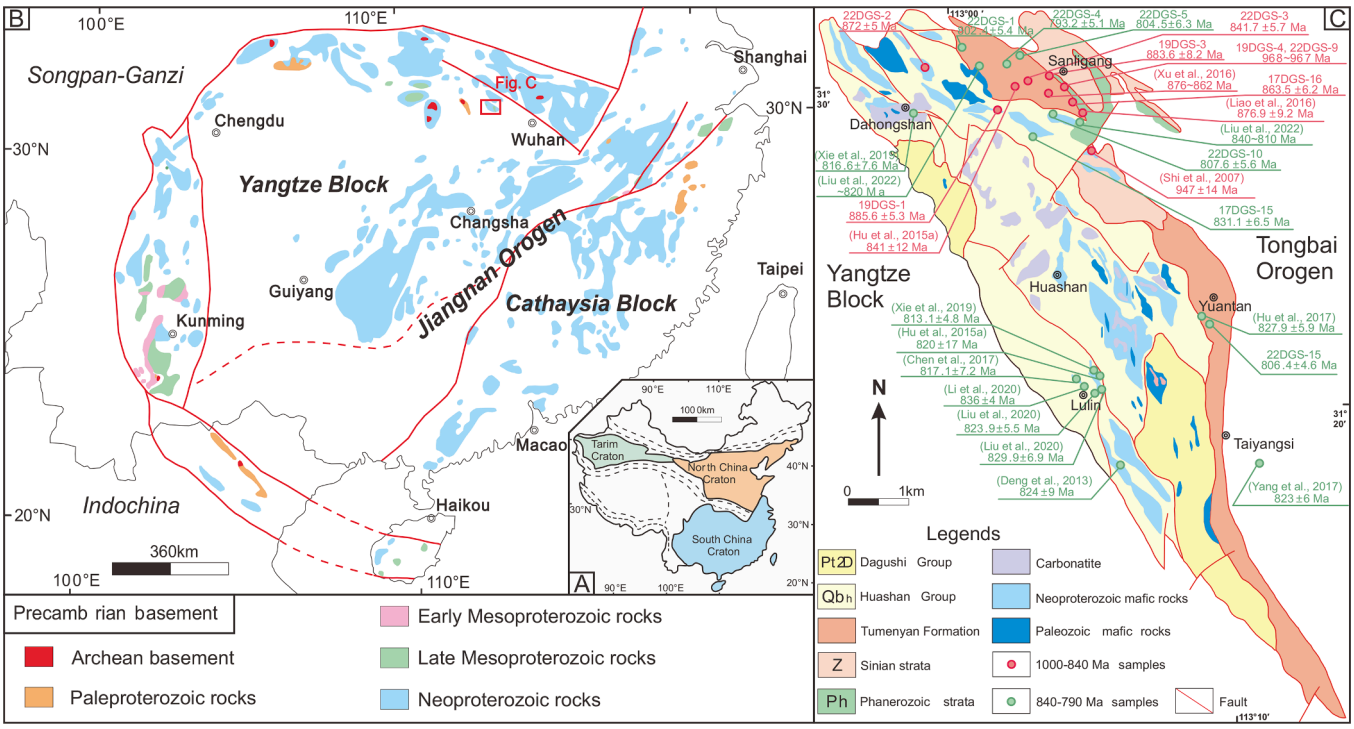

Fig. 1. Geological map of the South China Block and the study area. (A) Simplified geographic sketch map of China with major continental blocks. (B) Geological map of the South China Block showing the distribution of Precambrian geological units (Modified after Zhao and Cawood, 2012). (C) Geological map of the Dahongshan region on the northern margin of the Yangtze Block, showing the distribution of rock units and sampling locations (Modified after Hu et al., 2017). The literature-annotated sample points are referenced, while the remaining ones are from this work.

et al., 2021; Mulder et al., 2021). Currently widely accepted supercontinents include Nuna (ca. 2.1–1.3 Ga), Rodinia (ca. 1.3–0.8 Ga), and Pangea (0.6 Ga to present), from which the South China Block has played an important role since the formation of the Nuna supercontinent (Meert, 2012; Merdith et al., 2017; Cawood et al., 2018; Li et al., 2021; Zou et al., 2021).

The South China Block comprises of the Yangtze Block and the Cathaysia Block and is characterized by the outcropping of voluminous early to mid-Neoproterozoic igneous rocks on the periphery of the Yangtze Block (Zhao et al., 2018a; Huang et al., 2019; Yao et al., 2019; Le et al., 2021). Such rocks contain important information about continental growth and reworking, and they are particularly evident on the southeastern and western margins of the Yangtze Block, but are less on the northern margin. This may result from the Phanerozoic thick sediment coverage and tectonic overprinting of Early Paleozoic and Early Mesozoic collision and orogenesis with microblocks and the North China Craton. Therefore, the nature of Neoproterozoic magma source, tectonic evolution and dynamic process on the northern margin of the Yangtze Block is still unclear, although preliminary studies have been carried out on the Neoproterozoic igneous rocks in the area (Zhang et al., 2008, 2009; Zhao et al., 2013a, 2013b; Deng et al., 2013; Xu et al., 2016). One of the key issues is to decipher the detailed processes from orogenesis to rifting on the northern margin of the Yangtze Block and to define the tectonic transition between the two tectonic regimes. An in-depth study of this issue will help us better understand the history of continental accretion and breakup of the Yangtze Block and reconstruct its position in the Neoproterozoic supercontinent. This study focuses on the early to mid-Neoproterozoic igneous suites in the Dahongshan region of northern Yangtze Block, which is also close to the Archean continental nucleus (i.e., the Kongling Complex) of the Yangtze Block. Previous studies suggest that the Dahongshan Neoproterozoic igneous suites might contain accreted complex and rifting-related basaltic rocks (Hu et al, 2015a, 2015b, 2017; Liao et al., 2016; Xu et al., 2016; Liu and Zhao, 2019) and the detrital zircon from metasedimentary rocks in the Dahongshan area reveal a transition from oceanic arc to continental arc (Huang et al, 2021). Further detailed studies on the affinities and tectonic setting of the igneous suites undoubtedly play a crucial role in recognizing the periphery growth and reworking of the northern Yangtze Block and the geodynamic process in response to the convergence and divergence of the supercontinent Rodinia. In this work, a comprehensive study on the petrology, geochemistry, geochronology and isotopes of the Neoproterozoic igneous suites is presented. Our new data reveal a tectonic transition from arc accretion to within-plate extension at ca. 830 Ma in the northern Yangtze Block.

2. Geological setting

2.1. Regional geology

The South China Block is one of the oldest continents in east Asia, consisting of the Yangtze Block to the northwest and the Cathaysia Block to the southeast, separated by the Jiangnan Orogen (e.g., Wang et al., 2007, 2014). The Yangtze Block is separated from the North China Craton by the Qinling-Dabie-Sulu Orogen, from the Tibet plateau by the Songpan-Ganze Orogen and from the Indosinian Block by the Ailaoshan-Red River fault (Fig. 1A and B) (Zhao and Cawood, 2012). The rocks of Archean to Paleoproterozoic crystalline basement are sporadically exposed on the northern and southwestern margins of the Yangtze Block (Zhang et al., 2006a, 2006b; Gao et al., 2011; Chen et al., 2013; Li et al., 2014; Cawood et al., 2020; Cui, 2020; Cui et al., 2021), implying its long-term growth history. Most of these rocks underwent high-grade metamorphism at ca. 2.0–1.8 Ga, possibly related to the assembly of the Columbia supercontinent (Ling et al., 2000; Yin et al., 2013; Li et al., 2022). Till Neoproterozoic, the Yangtze Block was featured by a continuous arc-related magmatism during the period of 980–820 Ma, with abundant Neoproterozoic magmatic rocks and contemporary sedimentary sequences distributed on its periphery (Zhao et al., 2018a; Yao et al., 2019; Le et al., 2021; Li et al., 2021; Zou et al., 2021; Zhou

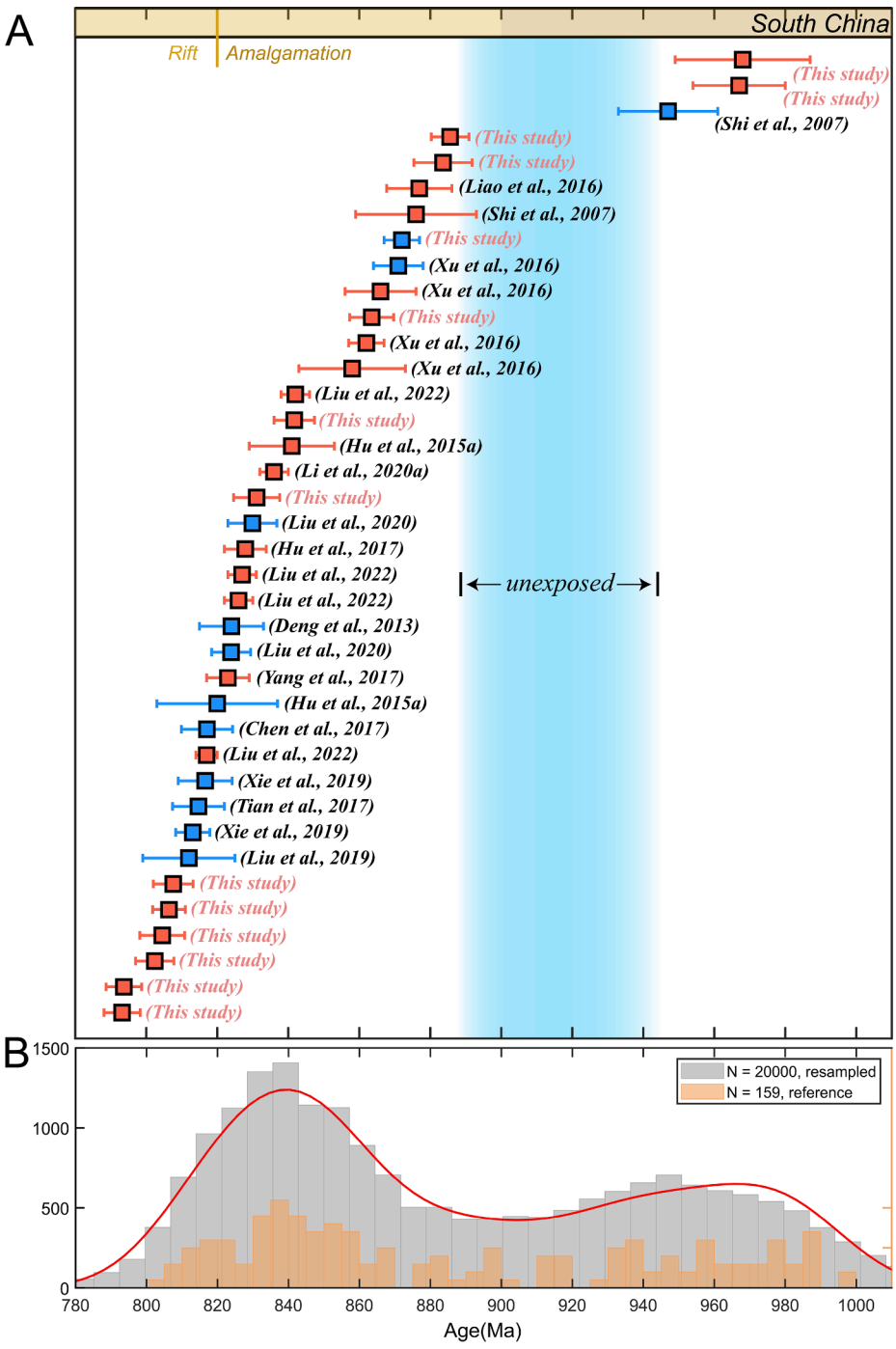

Fig. 2. Age distributions of the igneous rocks and detrital zircon from the sedimentary strata in the Dahongshan area. (A) Compiled U-Pb ages of igneous rocks in the Dahongshan area (Orange rectangle: intermediate-felsic rocks; Blue rectangle: mafic rocks). (B) Distribution of the compiled detrital zircon U-Pb ages in the Dahongshan area. The limit between amalgamation and dispersal for South China is set to an approximate time of complete assembly (Yan et al., 2019). The orange square represents immediate-felsic rocks and the blue square represents mafic rocks. The cited data of detrital zircon are from Yang et al. (2018), Li et al. (2020b) and Huang et al. (2021).

et al., 2022). However, the contemporary igneous rocks in its northern part have been poorly outcropped due to later tectonic overprinting. Previously reported volcanic rocks in the Suixian, Yaolinghe and Wudangshan regions and so forth on the northern margin of the Yangtze Block, strictly speaking, fall into the part of the South Qinling Belt. The igneous rocks actually on the northern Yangtze Block are mainly developed in the Kongling and Dahongshan regions, represented by the ca. 860–800 Ma Huangling granitoids and ca. 950–810 Ma mafic to felsic Dahongshan igneous suites, respectively (Shi et al., 2007; Zhang et al., 2008, 2009; Deng et al., 2013; Zhao et al., 2013a, 2013b; Wu et al., 2016; Xu et al., 2016; Xie et al., 2019; Liu et al., 2020). The available geochronological data evidently suggest that the Neoproterozoic igneous rocks in the Dahongshan region have a long magmatic span (see below).

2.2. Dahongshan igneous suites and sample details

The Dahongshan region comprises the Late Mesoproterozoic Dagushi Group and the overlying Neoproterozoic Huashan Group and a suites of Neoproterozoic igneous rocks (Fig. 1C). The Dagushi Group is characterized by stromatolite dolomite, indicating a stable shallow marine basin, whereas the Huashan Group is marked by sandstone and siltstone,

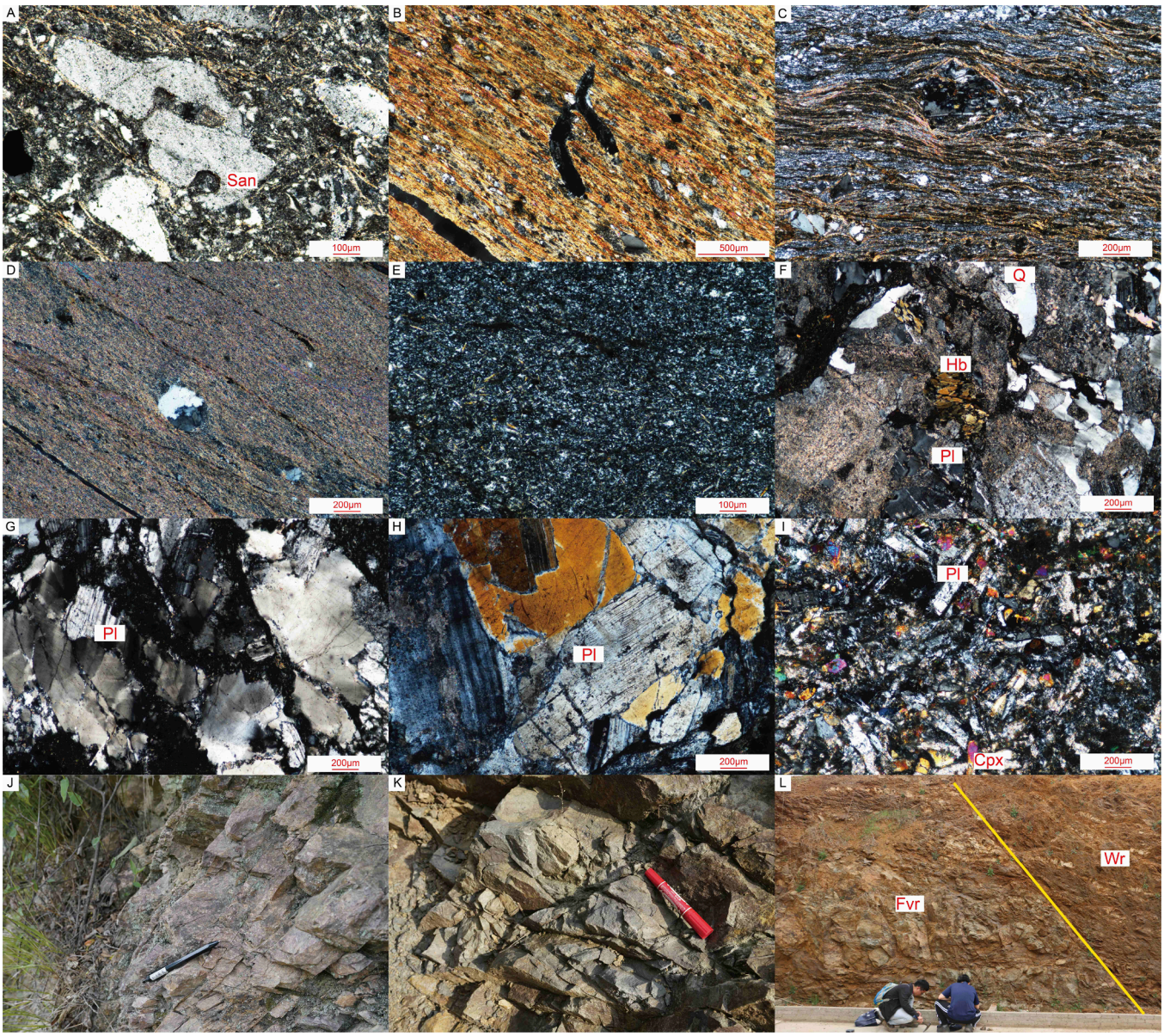

Fig. 3. Photomicrographs and field photos of the igneous rocks from the Dahongshan area. (A) Photomicrographs showing the corroded sanidine phenocryst observed in the rhyolite (sample 17DGS-15-1), (B) the "Y" type vitroclast seen in the tuff (sample 19DGS-1-4), (C-D) flow structure observed in tuff (sample 22DGS-5-1 and 22DGS-15-2), (E) very fined-grained felsic mineral assemblages (sample 19DGS-4-1), (F-H) the altered granodiorite mainly composed of plagioclase, quartz and hornblende (sample 22DGS-3-1, 17DGS-16-1 and 19DGS-3-3, respectively) and (I) the diabase mainly composed of clinopyroxene and plagioclase (sample 22DGS-2-3). Outcrop photographs showing the (J) rhyolite (sample 22DGS-1-1), (K) diabase (sample 22DGS-2-3) and (L) felsic volcanic rock (sample 19DGS-4-1). Abbreviations: Qz, quartz; San, sanidine; Pl, plagioclase; Hb: hornblende; Cpx, clinopyroxene; Fvr, felsic volcanic rock; Wr, wall rock.

implying the change of sedimentary settings (Li et al, 2016; Yang et al.,2018; Li et al., 2020a). The Dahongshan strata were dismembered by tectonic complexes and show evident fold deformation, accompanied by the thrust faults developed in the middle part of the study area (Hu et al., 2015a, 2015b; Yang, 2017). The geological structure was thought to be resulted from Neoproterozoic subduction-accretion process (Hu et al., 2017; Huang et al., 2021). In addition to tectonic complex, mafic–ultramafic rocks with ages ranging from 947 to 813 Ma were mainly exposed in the middle and southwest of the Dahongshan area (Shi et al., 2007; Deng et al., 2013; Tian et al., 2017; Chen et al., 2017; Xie et al., 2019; Liu et al., 2020). Moreover, previous work identified a NW-SE trending pyroclastic suites distributed along the northeastern margin of the Dahongshan region, mainly having ages of 871–828 Ma and being accompanied by mafic dykes, which were previously suggested to be the consequence of southwestward subduction of the Tongbai Block (Xu et al., 2016; Liao et al., 2016; Hu et al., 2015a, 2017; Yang, 2017; Huang et al., 2021). These igneous suites are jointly characterized by Neoproterozoic magmatic activities in northern Yangtze Block (Fig. 2).

In this study, fifteen felsic rocks (including 3 granodioritic rocks and 12 felsic volcanic rocks) and twenty mafic rocks (including 8 basalts, 4 gabbros and 8 diabases) were collected. The sampling localities are show in the Fig. 1C. Detailed GPS coordinates, mineral compositions and relevant information of the igneous rocks are summarized in the supplementary Table S1 of Appendix A. All these samples underwent variable degrees of alteration and low-grade metamorphism as evidenced by the observed chlorite and carbonates in thin section and only the immobile elements are discussed below (Fig. 3).

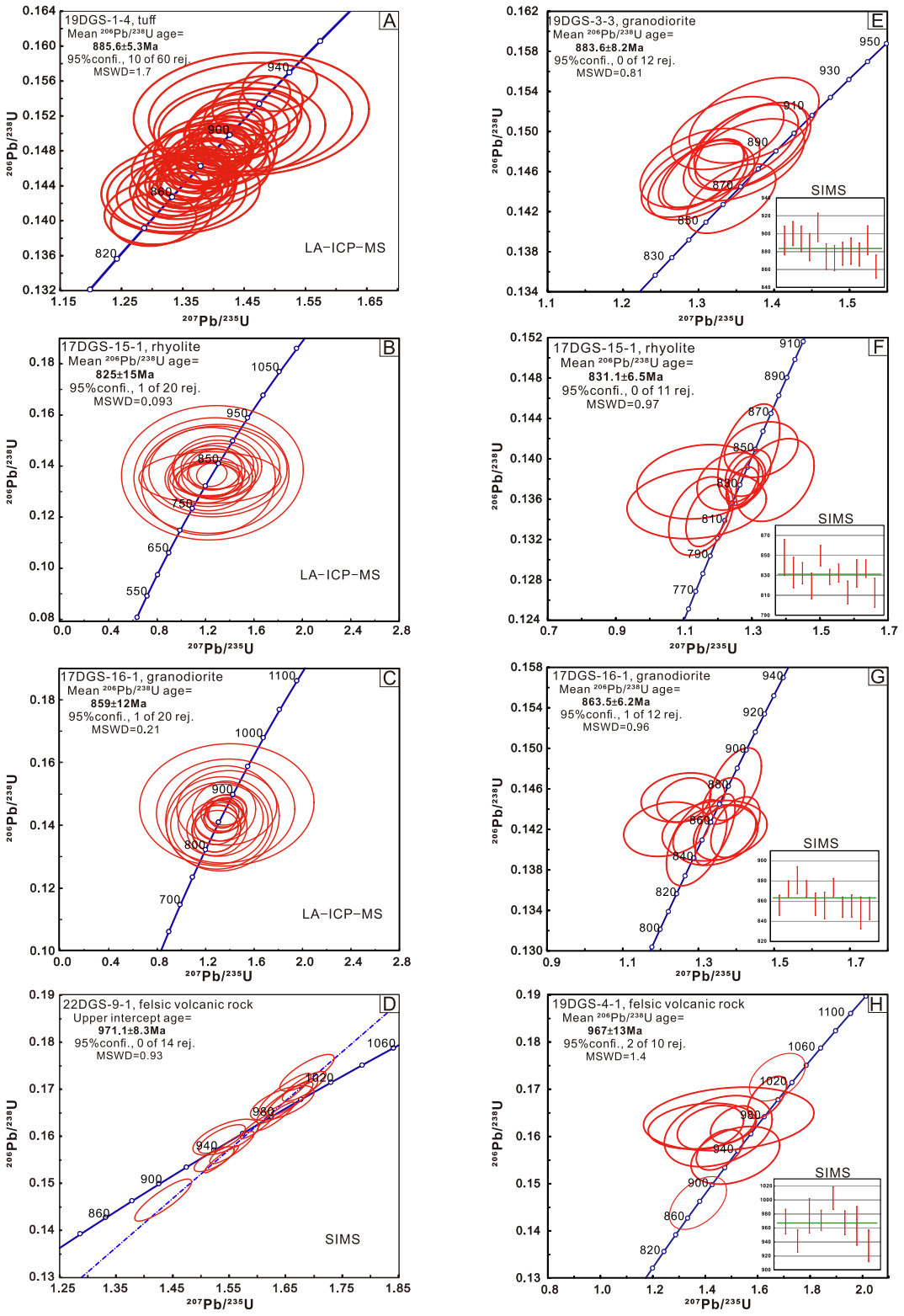

Fig. 4. Zircon U-Pb concordia diagrams for the igneous rocks from the Dahongshan area.

3. Analytical methods

3.1. Zircon U-Pb dating

Considering that the Dahongshan area may have contained a lot of accretionary complexes and variably lithological igneous rocks without clear contact relationships, we dated a large part of the collected samples to make sure the accurate temporal and geochemical linkages of these igneous rocks. Zircon crystals were separated using conventional heavy liquids and magnetic techniques, cast in epoxy, and polished to their mid-sections. In situ U-Pb isotope analyses were carried out guided by cathodoluminescence (CL) images and transmitted and reflected light

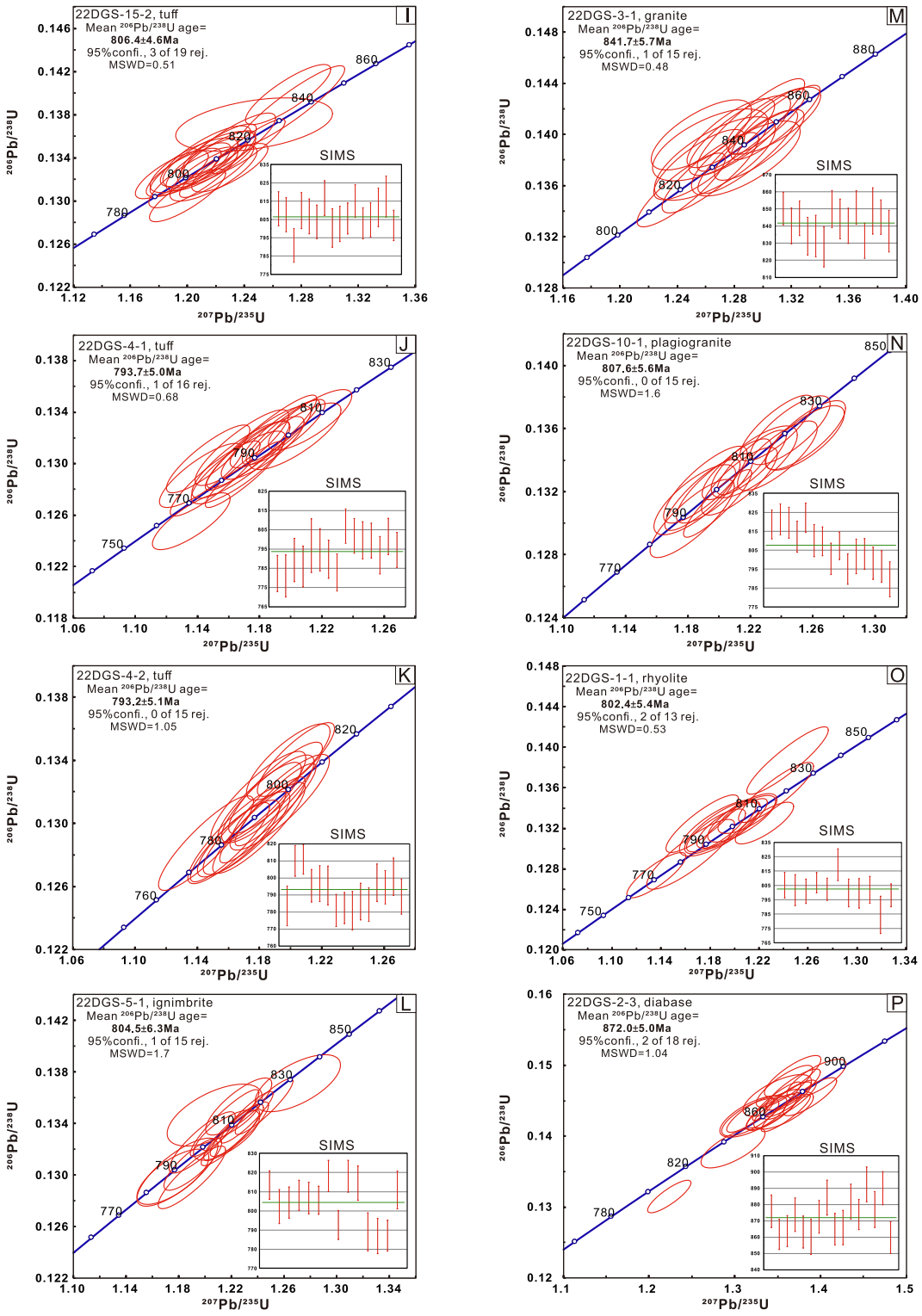

Fig. 4. (*continued*).

photographs.

3.1.1. LA-ICP-MS technique

Zircon U-Pb isotopic analysis for three samples (17DGS-15-1, 17DGS-16-1 and 19DGS-1-4) were conducted using an Agilent 7500a ICP-MS coupled to a GeoLas 193 nm laser ablation system at the State Key Laboratory for Mineral Deposits Research of Nanjing University (MiDeR-NJU), following the analytical methods of Jackson et al. (2004) and Wang et al. (2014). Ablation protocol employed a spot diameter of 32 μm at a 5 Hz repetition rate. Zircon standards GEMOC GJ-1 ($^{206}Pb/^{238}U$ age = 608.5 ± 1.5 Ma; Jackson et al., 2004) and Mud Tank ($^{206}Pb/^{238}U$ age = 732 ± 5 Ma; Black and Gulson, 1978) were used for isotopic mass fraction correction and age calculation. And the U-Pb dates were calculated from the raw signal data using the software GLITTER 4.4 (Griffin et al., 2008). The dating results are listed in Table S1 of Appendix B.

3.1.2. SIMS technique

Zircon U-Pb dating for four samples (17DGS-15-1, 17DGS-16-1, 19DGS-3-3 and 19DGS-4-1) was carried out using SHIRIMP II instrument at the Beijing SHRIMP Center, CAGS. The analytical procedures and conditions were described by Wang et al. (2021). All analyses were carried out with a spot size of 30 μm, the intensity of the primary O^{2-} ion beam between 4 and 8nA. The standards M257 (U = 840 ppm; Nasdala et al., 2008) and TEMORA-2 ($^{206}Pb/^{238}U$ age = 416.8 ± 1.3 Ma; Iles et al., 2015) were used to calculate U/Pb fractionations. Data processing was conducted using the SQUID and ISOPLOT programs (Ludwig, 2001, 2003). Uncertainties for weighted mean dates are quoted at the 95 % confidence level.

The remaining nine samples were conducted using a CAMECA IMS 1300-HR^3 instrument that was newly installed at the MiDeR-NJU. The instrument description and analytical procedure are similar to Li et al. (2009). The primary O_2^- ion beam spot is about 15 × 20 μm in size. Positive secondary ions were extracted with a 10 kV potential. Pb/U calibration was performed relative to zircon standard Plešovice ($^{206}Pb/^{238}U$ age = 337 Ma; Sláma et al., 2008); U and Th concentrations were calibrated against zircon standard 91500 (U = 81 ppm; Wiedenbeck et al., 1995). In order to monitor the external uncertainties of SIMS U-Pb zircon dating calibrated against Plešovice standard, an in-house zircon standard Qinghu ($^{206}Pb/^{238}U$ age = 159.5 ± 0.2 Ma; Li et al. 2013) was alternately analyzed as an unknown together with other unknown analyses. The detailed zircon U-Pb isotopic analyses are listed in Table S2 of Appendix B.

3.2. Zircon Hf isotopes

Zircon Lu-Hf isotopic analyses were carried out using a GeoLas 193 nm laser ablation system attached to a Neptune (Plus) MC-ICP-MS at the MiDeR-NJU. The analytical techniques are similar to those described in detail by Li et al. (2018a). A beam diameter of 44–50 μm was adopted at a repetition rate of 10 Hz and pulse energy density of 10.5 J/cm^2. Reference zircon standards Mud Tank and 91500 were used to monitor accuracy and precision of Hf isotope ratios and instrumental drift with respect to the Lu/Hf ratios. The decay constant for ^{176}Lu of 1.867 × 10^{-11} year^{-1} proposed by Scherer et al. (2001) was adopted in this work. The chondritic values of $^{176}Lu/^{177}Hf$ = 0.0336 ± 1 (2σ) and $^{176}Hf/^{177}Hf$ = 0.282785 ± 11 (2σ) (Bouvier et al., 2008) were applied to calculations of ε_{Hf} values. Analytical results of the Lu-Hf isotopic data are given in Table S3 of Appendix B.

3.3. Zircon O isotopes

Zircon O isotopic analyses were conducted using the CAMECA IMS 1300-HR^3 instrument at the MiDeR-NJU. A primary $^{133}Cs^+$ ion beam (2.8–3nA current and 20 keV total impact energy) was focused on the sample surface. A 5 × 5 μm raster was used in this study, and a normal-incidence electron gun was used for charge compensation. The signals of ^{16}O and ^{18}O were collected simultaneously using two Faraday cups at positions L'2 and H'2, respectively. The mass resolving power (MRP, M/ΔM), measured at 50 % peak height, was set at ~ 2500 to minimize isobaric interferences. To evaluate the reliability of the analytical protocols in this study, well-characterized zircon reference materials Penglai ($\delta^{18}O$ value: 5.31 ± 0.1 ‰; Li et al., 2010) and Qinghu ($\delta^{18}O$ value: 5.4 ± 0.2 ‰; Li et al., 2013) were also analyzed. The zircon O isotopic analyses are listed in Table S4 of Appendix B.

3.4. Whole-rock major and trace elements

Thirteen felsic samples and twenty mafic samples were prepared by crushing in an agate shatter box. Major elements were conducted using a Thermo ARL9900XP X-ray fluorescence spectrometer (XRF) at the MiDeR-NJU, with analytical precisions better than 2 % for all elements. Trace elements were analyzed using an ICP-MS (Finnigan MAT-Element 2) instrument at the MiDeR-NJU. The analytical precision for most elements is better than 5 %. The detailed analytical procedures were described by Li et al. (2018b). Whole-rock major and trace element analyses for all felsic rocks from the Dahongshan area are listed in the Table S1 of Appendix C.

4. Results

4.1. Zircon U-Pb age and Hf-O isotopes

A summary of in situ zircon U-Pb-Hf-O isotopic compositions are presented in the Appendix B. Representative cathodoluminescence (CL) images of zircon grains from analyzed rocks are shown in the Fig. S1 of Appendix D. Zircon grains from all the samples do have euhedral morphology, mainly showing oscillatory zoning or sector zoning and few of them have a thin dark overgrowth in CL images. All the analyzed zircon grains have Th/U ratios within the range of 0.31–2.9, significantly higher than the threshold of magmatic zircon. The zircon U-Pb concordia diagrams are shown in the Fig. 4.

Zircon grains from two felsic volcanic rocks (19DGS-4-1 and 22DGS-9-1) sampled from the same place yield consistent ages of a weighted average $^{206}Pb/^{238}U$ age of 967 ± 13 Ma (MSWD = 1.4, n = 8) and an upper intercept age of 971.1 ± 8.3 Ma (MSWD = 0.93, n = 14), respectively, which represent the ages of the oldest igneous rocks found in the Dahongshan area. The ca. 970 Ma magmatic zircon grains have similar $^{176}Hf/^{177}Hf$ ratios of 0.282434–0.282606, positive and high $\varepsilon_{Hf}(t)$ values of +8.0 to +14.7, and consistent young Hf isotope crustal model ages (T_{DM2} = 1.30–0.92 Ga). Only the dated zircon grains from the sample 22DGS-9-1 were analyzed for oxygen isotopes and the $\delta^{18}O$ values vary from 5.59 ‰ to 6.23 ‰, slightly higher than the mantle zircon value of 5.3 ± 0.6 ‰ (2σ; Valley et al., 1998).

Fifty spot analyses for the tuff sample (19DGS-1-4) give concordant U-Th-Pb dates and yield a weighted average $^{206}Pb/^{238}U$ age of 885.6 ± 5.3 Ma (MSWD = 1.7, n = 50). Similarly, zircon grains from the granodiorite sample (19DGS-3-3) give a weighted average $^{206}Pb/^{238}U$ age of 883.6 ± 8.2 Ma (MSWD = 0.81, n = 12). Twenty-nine dated zircon grains from the sample 19DGS-1-4 were analyzed for in-situ Hf isotopes. Most of them have initial $^{176}Hf/^{177}Hf$ ratios of 0.282510–0.282578 and high $\varepsilon_{Hf}(t)$ values of +9.3 to +12.3 with T_{DM2} = 1.15–1.01 Ga, except for several analyses showing a bit enriched $\varepsilon_{Hf}(t)$ values of +3.3 to –2.3 and T_{DM2} = 1.92–1.54 Ga. Zircon grains from the sample 19DGS-3-3 have similar positive $\varepsilon_{Hf}(t)$ values of +9.7 to +11.5 and young T_{DM2} = 1.14–1.04 Ga, and their $\delta^{18}O$ values of 5.88–6.34 ‰ are also slightly higher than typical mantle zircon.

Eleven analyses were conducted on zircon grains from the granodiorite sample (17DGS-16-1), yielding a weighted average $^{206}Pb/^{238}U$ age of 863.5 ± 6.2 Ma (MSWD = 0.96, n = 11). The dated grains have positive $\varepsilon_{Hf}(t)$ values from +7.3 to +10.1 and initial $^{176}Hf/^{177}Hf$ ratios of 0.282438–0.282516 with T_{DM2} = 1.29–1.11 Ga. They have $\delta^{18}O$ values of 5.9–6.6 ‰, similar to the values of the above-mentioned zircon.

Fourteen spot analyses for the granite sample (22DGS-3-1) yield a weighted average $^{206}Pb/^{238}U$ age of 841.7 ± 5.7 Ma (MSWD = 0.48, n = 14). And these zircon grains exhibit elevated $\delta^{18}O$ values of 6.6–6.89 ‰ relatively to the above-mentioned igneous zircon.

The zircon grains from the rhyolite sample (17DGS-15-1) give a weighted average $^{206}Pb/^{238}U$ age of 831.1 ± 6.5 Ma (MSWD = 0.97, n = 11). They have negative $\varepsilon_{Hf}(t)$ values of –5.7 to –0.8 and initial $^{176}Hf/^{177}Hf$ ratios of 0.282126–0.282253 with older T_{DM2} = 2.09–1.78 Ga. Twelve SIMS O isotope spots on these grains yield $\delta^{18}O$ values between 3.81 ‰ and 4.63 ‰ with an average value of 4.19 ‰, lower than the value of typical mantle zircon.

Zircon grains from one plagiogranite (22DGS-10–1), one tuff (22DGS-15-2), one ignimbrite (22DGS-5-1) and one rhyolite (22DGS-1-1) do show similar weighted average $^{206}Pb/^{238}U$ ages of 807.6 ± 5.6 Ma (MSWD = 1.6, n = 15), 806.4 ± 4.6 Ma (MSWD = 0.51, n = 16), 804.5 ± 6.3 Ma (MSWD = 1.7, n = 14) and 802.4 ± 5.4 Ma (MSWD = 0.53, n

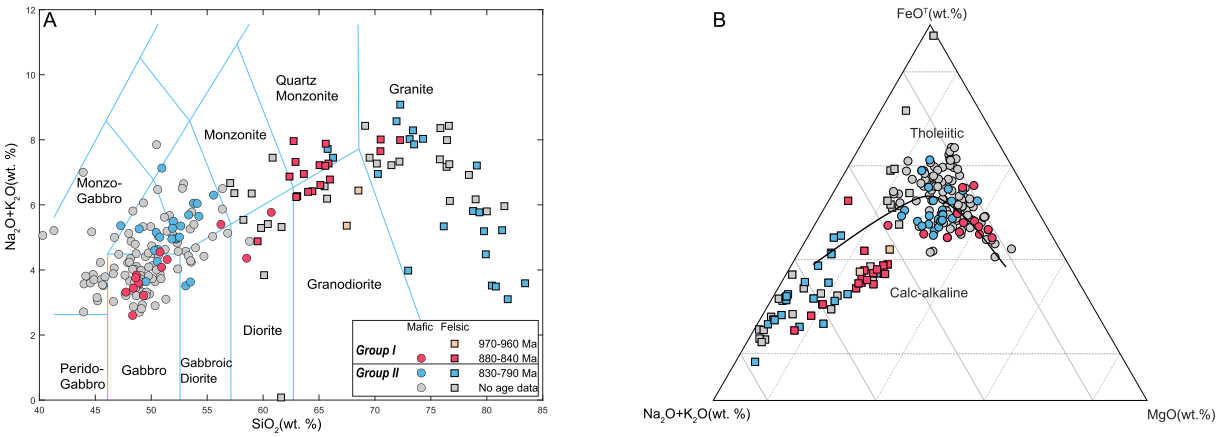

Fig. 5. Rock classification diagrams for the igneous rocks from the Dahongshan area. (A) Total alkali vs. silica diagram. (B) ($Na_2O + K_2O$)–FeO^T–MgO (AFM) plot from Irvine and Baragar (1971). Data sources are from Dong et al. (1999), Dong (2004), Shi et al. (2003, 2005), Deng et al. (2013), Hu et al. (2015a, 2017), Liao et al. (2016), Xu et al. (2016), Chen et al. (2017), Yang (2017), Xie et al. (2019), Liu and Zhao (2019), Liu et al. (2020, 2022) and this study.

= 11), respectively. These samples do have consistent Hf and O isotopic compositions with significant positive $\varepsilon_{Hf}(t)$ values of +10.5 to +15.3, elevated initial $^{176}Hf/^{177}Hf$ ratios of 0.282564–0.282706, and mantle-like $\delta^{18}O$ values between 4.61 ‰ and 5.84 ‰.

The zircon grains from two tuff samples (22DGS-4-1 and 22DGS-4–2) give consistent weighted average $^{206}Pb/^{238}U$ ages of 793.7 ± 5.0 Ma (MSWD = 0.68, n = 15) and 793.2 ± 5.1 Ma (MSWD = 1.05, n = 15), respectively. These dated zircon grains also exhibit consistent mantle-like $\delta^{18}O$ values of 5.2 ‰–6.1 ‰.

Only one mafic sample (22DGS-2-3) was successful in zircon separation in this study and the zircon grains yield a weighted $^{206}Pb/^{238}U$ age of 872 ± 5 Ma (MSWD = 1.04, n = 16), which can be interpreted as the crystallization age of the gabbro. These zircon grains have $\delta^{18}O$ values of 6.1 ‰–6.6 ‰, slightly higher than the normal mantle zircon value. Eleven dated zircon grains were further selected for in-situ Hf isotope analysis and show positive $\varepsilon_{Hf}(t)$ values of +9.3 to +13.5, high initial $^{176}Hf/^{177}Hf$ ratios of 0.282497–0.282623, and young T_{DM1} ages of 1.04–0.87 Ga.

It should be noted that among all the obtained dating analyses, only the U-Pb dates within 5 % discordance were adopted for age calculations.

4.2. Whole-rock major and trace elements

Thirty-three samples including thirteen intermediate-felsic and twenty mafic rocks were analyzed for whole rock major and trace element compositions, with detailed analytical results listed in the Table S1 of Appendix C. The rocks show wide ranges of SiO_2 and alkali contents (Fig. 5A). Among them, the felsic rocks from the Dahongshan area can be divided into two groups: one formed at ca. 970–840 Ma, and the other crystallized at ca. 830–790 Ma. The older group shows similar whole-rock major element contents, characterized by intermediate to high SiO_2 (62.7–68.5 wt %), Al_2O_3 (14.2–16.2 wt %), and low MgO contents (2.18–3.29 wt %) and K_2O/Na_2O ratios (0.02–0.54) and aluminum saturation index (ASI) (0.85–1.33). They are also characterized by enrichments in light rare earth elements (LREEs), flat heavy rare earth elements (HREE) patterns, and the absence of obvious Eu anomalies (Fig. 6A-D). In comparison, the younger group have relatively high SiO_2 (65.8–79.3 wt %, except for two at 81.9–83.4 wt %) and K_2O/Na_2O ratios (0.41–55.2) and ASI (1.01–3.17), variable Al_2O_3 (10.3–19.7 wt %) and low MgO contents (0.23–2.28 wt %). This group displays variable enrichments in LREEs and high concentrations in HREEs with evident negative anomalies of Eu and Sr-P-Ti (Fig. 6E and F). In the FeO^T-ALK (alkali)-MgO diagram, the two groups of felsic rocks mostly plot in the calc-alkaline field (Fig. 5B). The mafic rocks of the two groups show wide ranges of SiO_2 (45.6–60.7 wt %) (including andesitic basalts), TiO_2 (1.14–3.86 wt %), Al_2O_3 (12.5–17.0 wt %), MgO (2.65–10.1 wt %) with Mg# in 29.3–63.6 and total alkali (3.21–5.62 wt %) contents. The basaltic rocks of this study exhibit variable REE patterns between typical N-MORB (normal middle ocean ridge basalt) and E-MORB (enriched middle ocean ridge basalt) with $La/Yb_{(N)}$ (the subscript "$_N$" denotes normalizing by chondrite) ratios ranging from 0.89 to 3.25 (Fig. 6G–J). Most of them exhibit variable anomalies of LILE (large ion lithophile element) and slight Nb-Ta negative anomalies. And the two groups of mafic rocks from early to late fall mainly within the calc-alkaline and tholeiitic fields, respectively (Fig. 5B).

All the samples have experienced variable degrees of alteration and low-grade metamorphism with loss-on-ignite (LOI) values ranging from 1.74 to 6.76 wt %. The primordial compositions of relative mobile elements, such as large ion lithophile elements (LILE) (e.g., Rb, Ba, Sr, and K), may have been modified by these later processes and are not used in the following discussion on petrogenesis and tectonic setting discriminants of mafic rocks. The assessment of the effect of alteration and metamorphism on the mafic rocks has revealed that the immobile elements of REEs and HFSEs employed in this study are reliable (Fig. S1 of Appendix E).

5. Discussion

5.1. A time span of ca. 180 Myr magmatic activities in the Dahongshan area

Whatever the pioneer study of the Dahongshan igneous rocks in the last century (e.g., Dong et al., 1999), due to the lack of enough accurate dating results, the chronology of the igneous rocks in the area and the corresponding tectonic evolution are difficult to constrain. Shi et al. (2007) first reported SHRIMP zircon U-Pb ages for the Yangjiapeng gabbro (947 ± 14 Ma) and Sanligang granite (876 ± 17 Ma) in the Dahongshan area, which suggest that at least some of the Dahongshan igneous rocks were formed at Early Neoproterozoic. Subsequent studies reported additional U-Pb age data of igneous rocks from ca. 870 Ma to ca. 810 Ma in the area (Fig. 2A). The new age data of this study evidently expand the age span of the magmatic activities in the Dahongshan area and partly fill the age gaps of previous data (Fig. 2A). Combined together, the compilation of published and our new geochronological data suggests a protracted magmatism from ca. 970 Ma to ca. 790 Ma in northern Yangtze Block. The igneous activities are generally continuous, except a ca. 60 Myr time gap (magmatic lull) between 947 Ma and 885 Ma (Fig. 2). We use the Monte Carlo resampling method to resample the age of detrital zircon for 20,000 times, which makes more reliable and

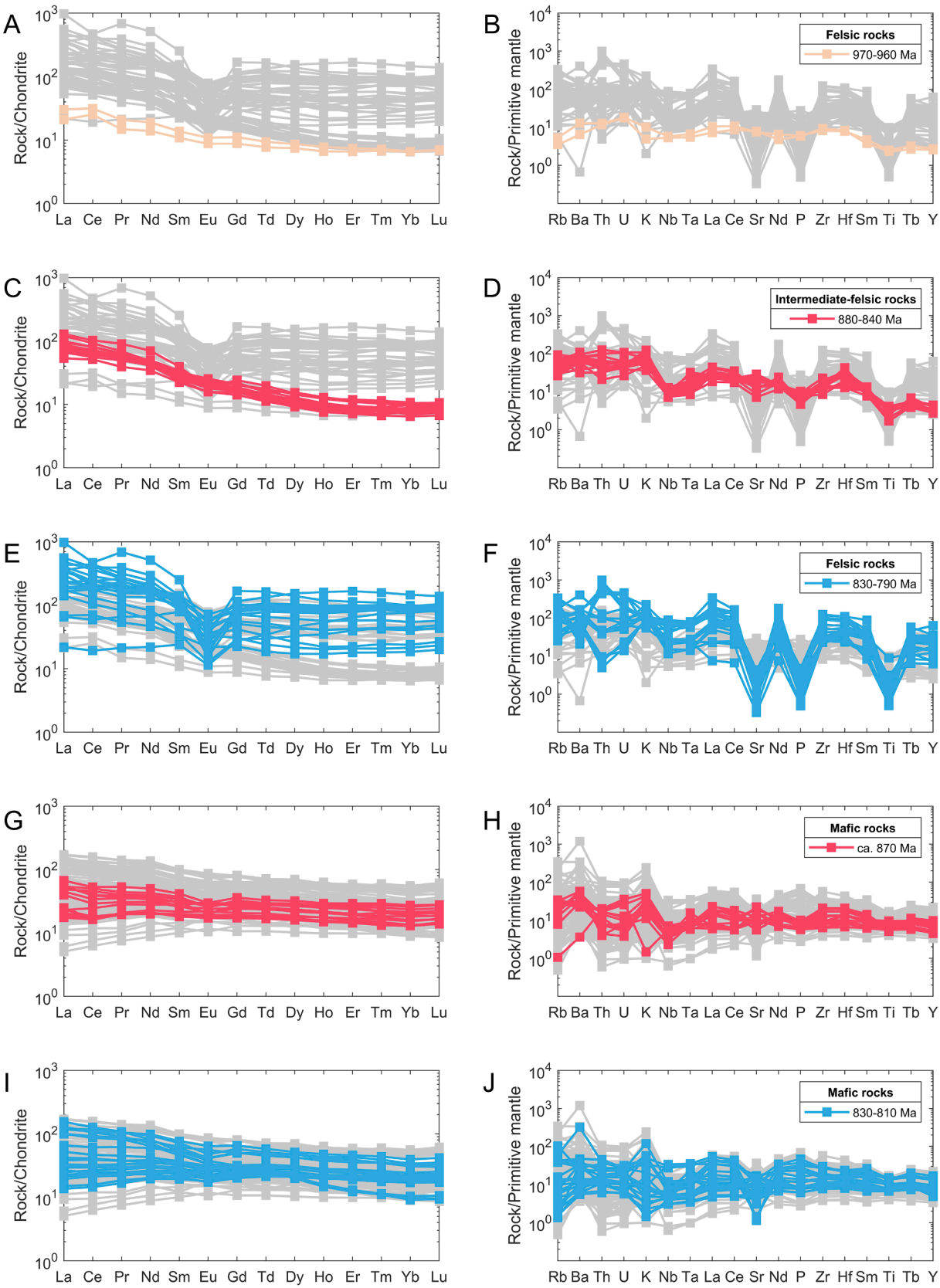

Fig. 6. Chondrite-normalized REE distribution patterns and primitive mantle-normalized trace element spidergrams for dated intermediate-felsic rocks and mafic rocks from the Dahongshan area, respectively. All intermediate-felsic rocks and mafic rocks are marked together by grey lines. Data sources are the same as those in Fig. 5. Chondrite and primitive-mantle data are from Sun and McDonough (1989).

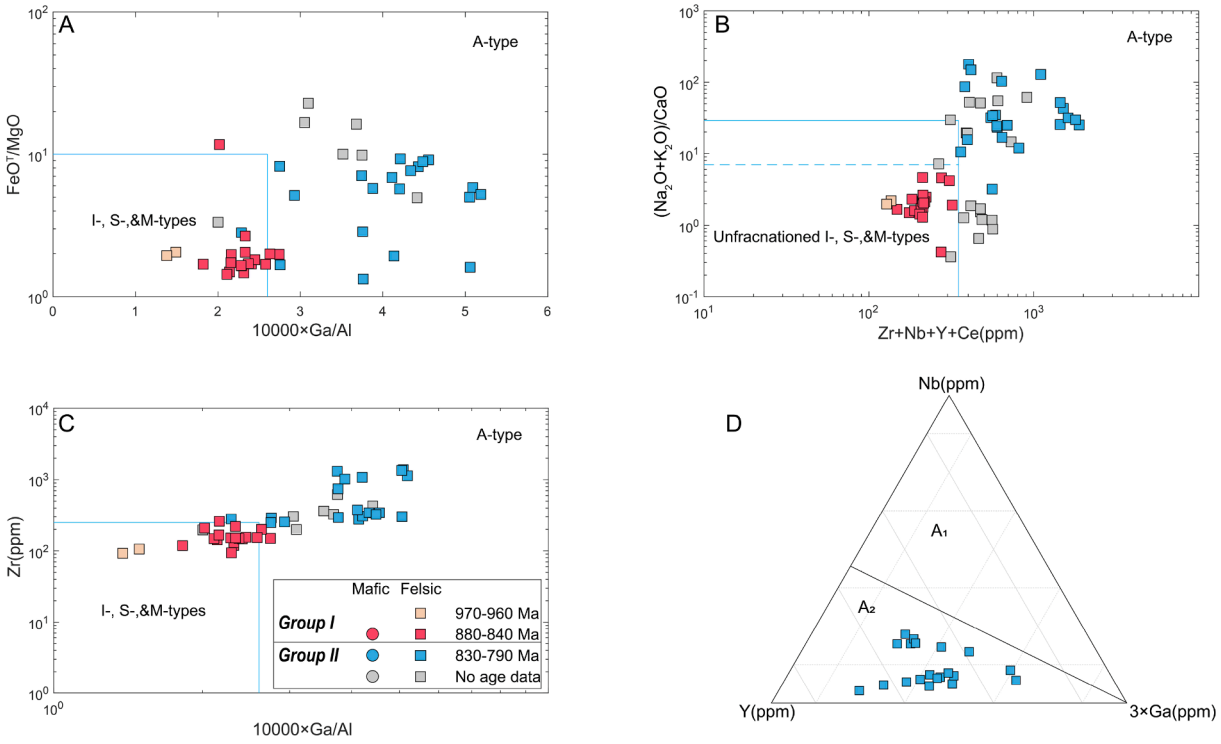

Fig. 7. Geochemical diagrams for the intermediate-felsic rocks. Plots of (A) FeO^T/MgO vs. 10000 × Ga/Al and (B) $(Na_2O + K_2O)/CaO$ vs. Zr + Nb + Y + Ce and (C) Zr vs. 10000 × Ga/Al for the intermediate-felsic rocks (after Whalen et al., 1987). (D) Y–Nb–3 × Ga ternary diagram showing the classification of A_2-type felsic rocks (after Eby, 1992). Data sources are the same as those in Fig. 5.

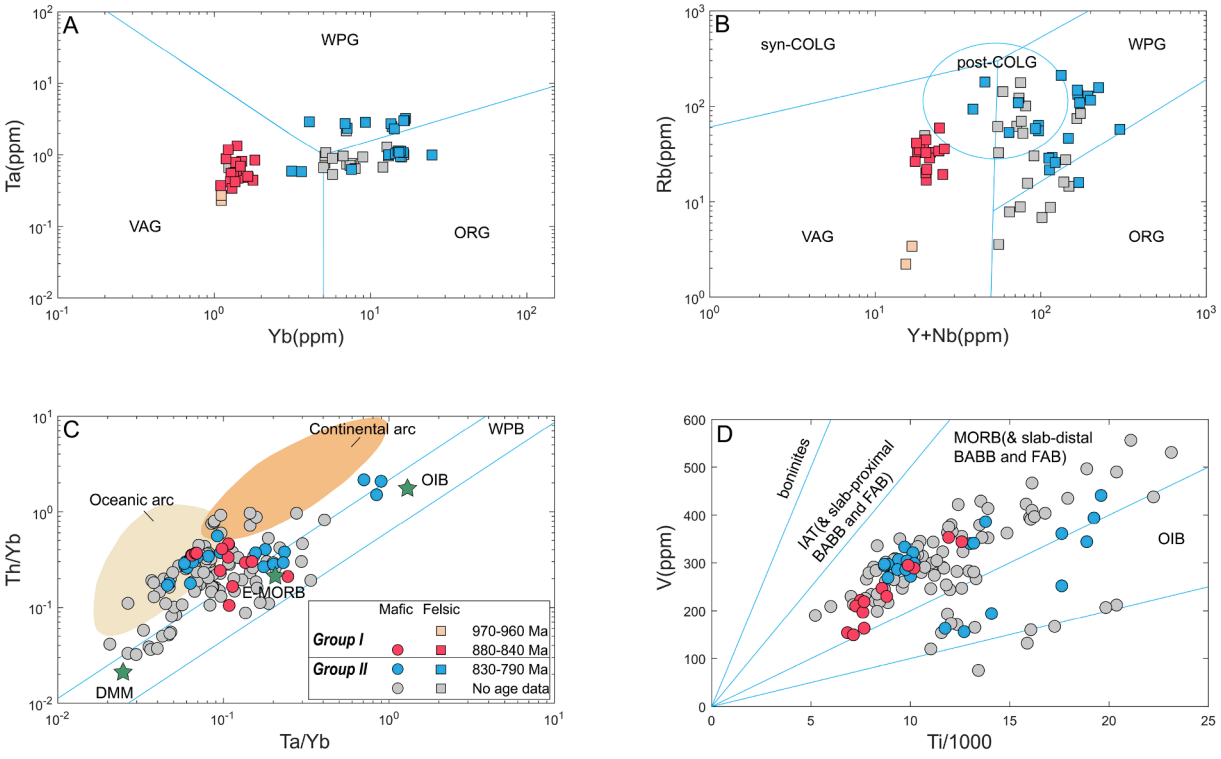

Fig. 8. Tectonic setting discrimination diagrams for the Dahongshan igneous suites. (A) Plot of Ta vs. Yb for intermediate-felsic samples (after Pearce et al., 1984). (B) Rb vs. Yb + Nb diagram for intermediate-felsic samples (after Pearce et al., 1984). (C) Th/Yb vs. Ta/Yb discriminant diagram for mafic rocks (after Pearce, 1982; Shu et al., 2019). (D) The V–Ti diagram for mafic rocks (after Pearce, 2014). Data sources are the same as those in Fig. 5.

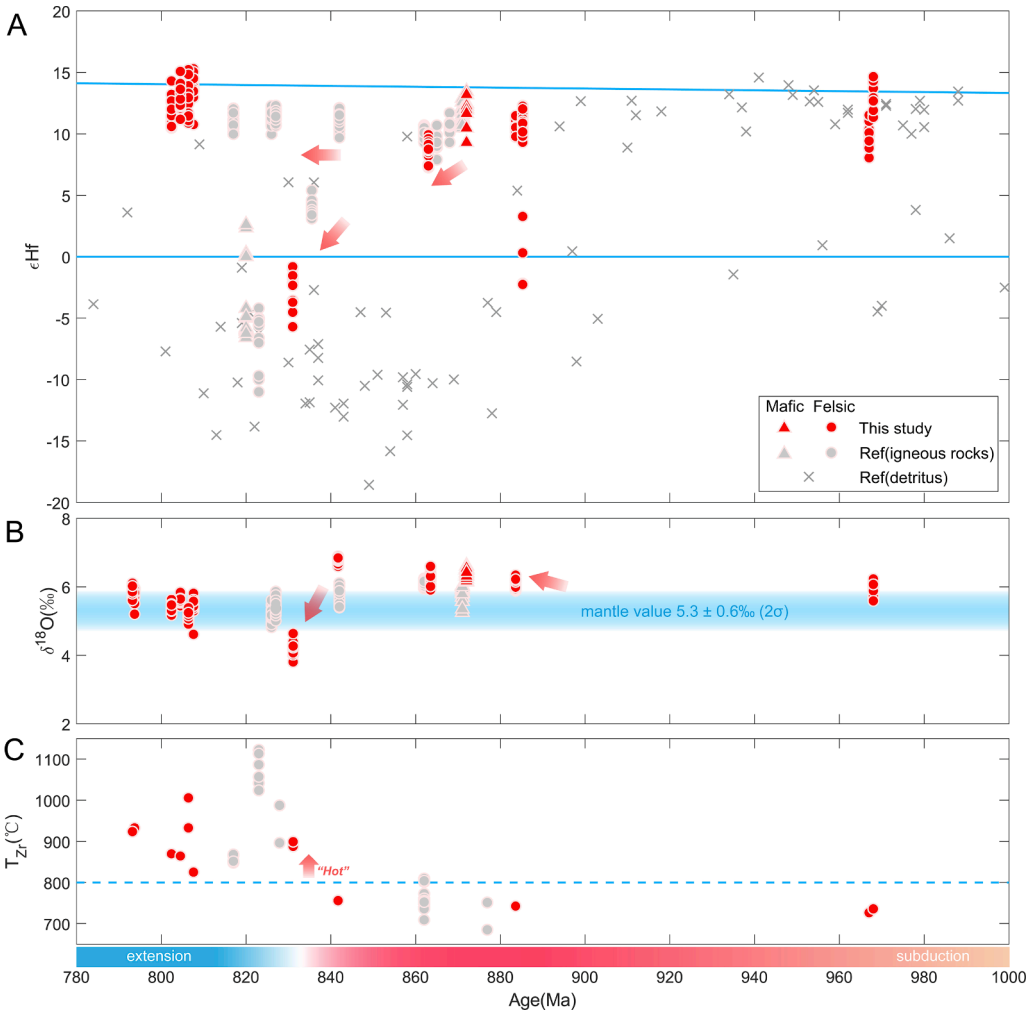

Fig. 9. Zircon Hf-O isotope and zircon saturation temperature with time. (A) Hf isotope compositions of zircon from igneous and sedimentary rocks. (B) Zircon $\delta^{18}O$ values versus U-Pb ages from igneous rocks. (C) Variations in zircon saturation temperature (T_{Zr}) of intermediate-felsic rocks with time (The calculation is detailed in Miller et al., 2003). Data sources are the same as those in Fig. 2.

obvious results. The resampled age pattern of the detrital zircon intuitively shows continuous distribution with two age peaks at ca. 970 Ma and ca. 840 Ma and a mild trough between ca. 920 Ma and ca. 880 Ma (Fig. 2B). The continuous age data for the resampled detrital zircon and the mild trough revealed in Fig. 2B may suggest unactive magmatism during this period and/or simply sampling bias. Anyhow, it's no doubt a time span of ca. 180 Myr continuous magmatism has developed in the Dahongshan area with a magmatic flare-up at ca. 840 Ma.

5.2. *Tectonic transition of the Dahongshan igneous suites*

The newly compiled ca. 970–790 Ma igneous rocks in the Dahongshan area have shown a wide range of SiO_2 contents (supplementary Table S1 of Appendix C), exhibiting a continuous geochemical spectrum extending from basalt/gabbro to rhyolite/granite (Fig. 5A). The temporal changes in the nature of magmatism are evident in the varying whole-rock compositions (Figs. 6 and 7), and the Dahongshan igneous suites can be roughly divided into two age groups as aforementioned in the geochemistry section.

5.2.1. *Group I (ca. 970–840 Ma)*

In terms of trace elements, most of the Group-I felsic suites display enrichment of LREEs relative to HREEs, enrichment of LILEs (e.g., Rb, Ba and K) and depleted in HFSEs (e.g., Nb, Ta and Ti) (Fig. 6). In the Yb vs. Ta and Y + Nb vs. Rb diagrams, the Group-I felsic suites all fall within the volcanic arc granites (VAG) field (Fig. 8A, B), which, combined with the existence of hornblende in some samples and the absence of aluminum-rich minerals in all samples, further supporting a subduction-related origin. Previous studies have also proposed that the 880–860 Ma Sanligang granitoids and mafic dykes were generated in a Neoproterozoic arc setting (Liao et al., 2016; Xu et al., 2016). The 872 ± 5 Ma gabbro in this study shows similar arc-like geochemical signatures with contemporary mafic dykes reported by Xu et al. (2016) (Figs. 6 and 8). In particular, the ca. 880–840 Ma mafic rocks all show clearly depletions of Nb and Ta relatively to neighboring elements in spider diagrams (Fig. 6H) and plot in the subduction-related regions (Fig. 8C, D). Moreover, the ca. 855 Ma Huangling tonalite-trondhjemite-granite series were also suggested to be formed in a continental arc setting defined by an oceanic-slab subduction beneath the northern margin of the Yangtze Block (Zhao et al., 2013a, 2013b), roughly consistent with the contemporary tectonic process occurred in the Dahongshan area.

In this work, the oldest ca. 970 Ma felsic volcanic rocks are characterized by weak enrichments of LREEs with $La/Yb_{(N)}$ ratios of 3.25–4.63, less obvious LILE, HFSE anomalies and they clearly plot within VAG field as well, which may be related to the early stage of the subduction and possibly reworking of juvenile crust or fractionation of mafic to intermediate magmas. Considering that these rocks do not resemble the contemporaneous Xiwan plagiogranites on the southeastern margin of the Yangtze Block (Sun et al., 2020), they are more likely to be resulted from the fractional crystallization of coeval mafic to intermediate melts.

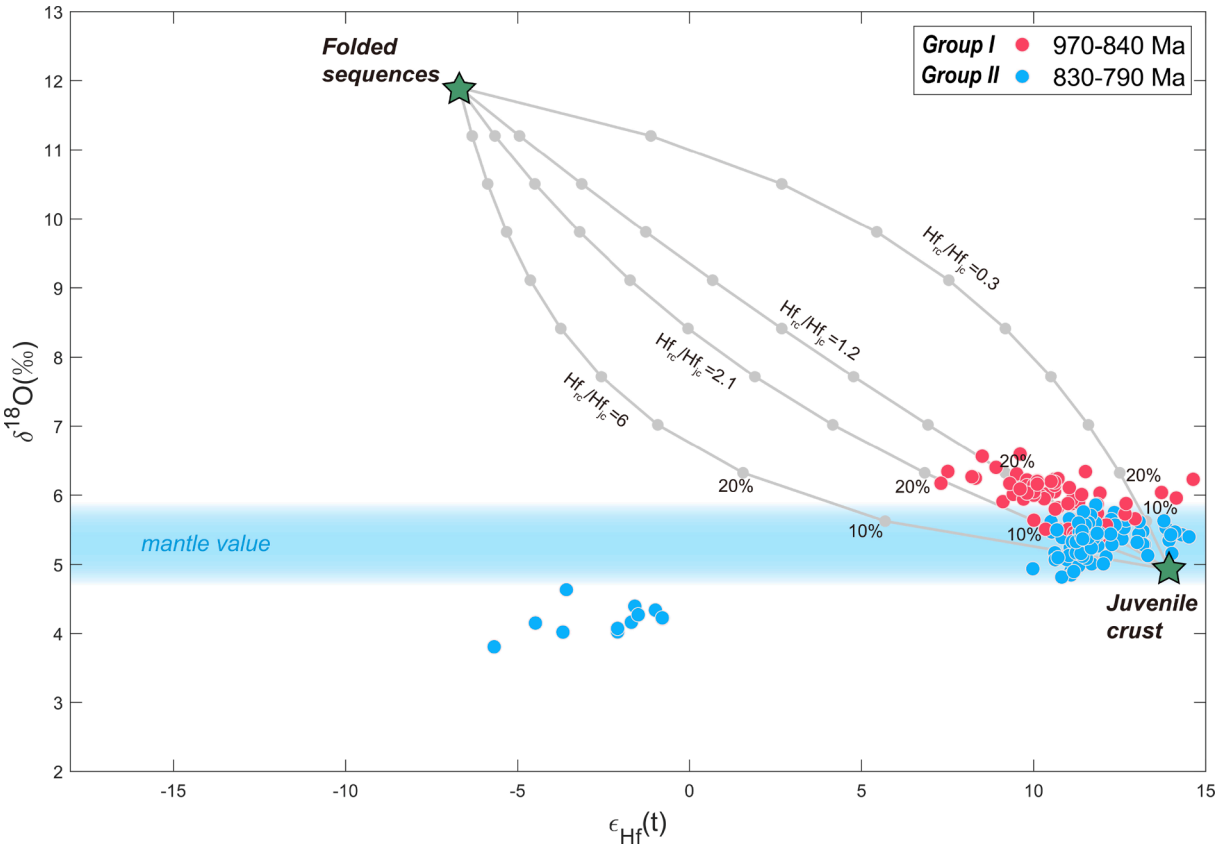

Fig. 10. Plot of in-situ zircon $\varepsilon_{Hf}(t)$ and $\delta^{18}O$ of the Dahongshan felsic suites, showing two-component mixing between folded sequences (reworked crust) and juvenile crust. Mixing curves are drawn to fit data points and to reflect the differences in Hf content ratios between reworked crust (rc) and juvenile crust (jc) end-members. Folded sequences with $\varepsilon_{Hf}(820\ Ma) = -6.7$ and $\delta^{18}O = 11.9$ ‰ are referred to Wang et al. (2013). Juvenile sequences with $\varepsilon_{Hf}(970\ Ma) = 13.9$ and $\delta^{18}O = 4.9$ ‰ are referred to Lu et al. (2020).

Recently, the Xiaoxikou metasedimentary rocks of the Miaowan area in the Kongling complex were recognized and interpreted to have been deposited in a fore-arc basin during a ca. 970–900 Ma subduction of the oceanic plate (Lu et al., 2020). This subduction event is temporally consistent with our new results, supporting that the subduction has begun at ca. 970 Ma in northern Yangtze Block and continued to ca. 840 Ma.

5.2.2. Group II (ca. 830–790 Ma)

The term "A-type granite" was coined by Loiselle and Wones (1979) to represent granitic rocks with characteristic alkaline, anorogenic and anhydrous feature. A-type granites generally have high alkaline contents, K_2O/Na_2O and $FeO^T/(FeO^T/MgO)$ ratios, and enrichment in incompatible elements such as REEs (except Eu) and HFSEs (e.g. Ga, Zr, Ce and Y) and are characterized by pronounced anomalies of Sr, P and Ti due to high degrees of mineral fractionation (Bonin, 2007).

The Group-II felsic suites have most of the characteristics of A-type granites, including moderate to high total alkalis ($K_2O + Na_2O$ = 3.10–9.08 wt %), generally high concentrations of total REE and HFSE with significant depletions of Eu, Sr, P, and Ti (Fig. 6E, F). Additionally, most of these samples have high Ga/Al ratios over 2.6 (Fig. 7A, C), Zr + Nb + Y + Ce (382–1790 ppm) (Fig. 7B) and $(Na_2O + K_2O)/CaO$ ratios. Nearly all the Group-II felsic suites plot in the A-type granite field in various discriminating diagrams (Fig. 7A-C), distinct from the Group-I felsic suites. The Group-II felsic rocks are further classified as A_2 granites according to their high Y/Nb ratios (Fig. 7D).

The geochemistry of Group-II felsic rocks also provides implications for their tectonic settings. Most of them plot in the within-plate granite (WPG) and oceanic-ridge granite (OGR) fields on the tectonic discriminant diagrams of Yb vs. Ta and Y + Nb vs. Rb (Fig. 8A, B), significantly different from the Group-I felsic rocks. In addition, all of the Neoproterozoic Dahongshan igneous suites show an evident increase of the calculated zircon saturation temperatures (T_{Zr}) from Group- I to Group-II felsic rocks. After ca. 830 Ma, the T_{Zr} value dramatically increases up to 1000 °C, resembling the high-temperature granite (Miller et al., 2003) (Fig. 9). This temperature difference implies that additional advective heat may have contributed to the formation of the Group-II felsic rocks, and this undoubtedly needs an extensional tectonic setting.

Coeval mafic magmatism provides evidence for the tectonic extension during the formation of Group-II felsic rocks. Although the Group-II mafic rocks share similar source distribution characteristics with Group-I mafic rocks, additional OIB- like mafic rocks have emerged (Fig. 8C and D). And the 830–810 Ma mafic samples are characterized by enrichments of incompatible elements like TiO_2 (1.39–3.86 wt %) without pronounced negative Nb-Ta-Zr-Hf anomalies. These mafic rocks have high Ti/V (29.2–81.4) and Zr/Y (2.74–8.63) ratios, features similar to within-plate basalts formed in a continental rift. Some of these mafic rocks are also locally associated with contemporary A_2-type rhyolites, forming a bimodal volcanic suite that is typical of an extensional setting. There are additional reasons to favor a within-plate setting rather than back-arc setting developed in the Dahongshan area after ca. 830 Ma: (1) the Middle Neoproterozoic sedimentary basins in the northern margin of the Yangtze Block show rift basin characteristics (Deng, 2013); (2) there is no evidence to support the continuous subduction along the northern margin of the Yangtze Block after ca. 800 Ma, argue against the possibility of a back-arc setting; (3) the existence of low-$\delta^{18}O$ zircon found in core domains of the HP (high pressure)-UHP Triassic metamorphic rocks in the Dabie orogen also supports a Neoproterozoic rifting setting on the northern margin of the Yangtze Block (Zheng et al., 2008). The rift-related magmatism was also recorded by the 816–801 Ma Huangling

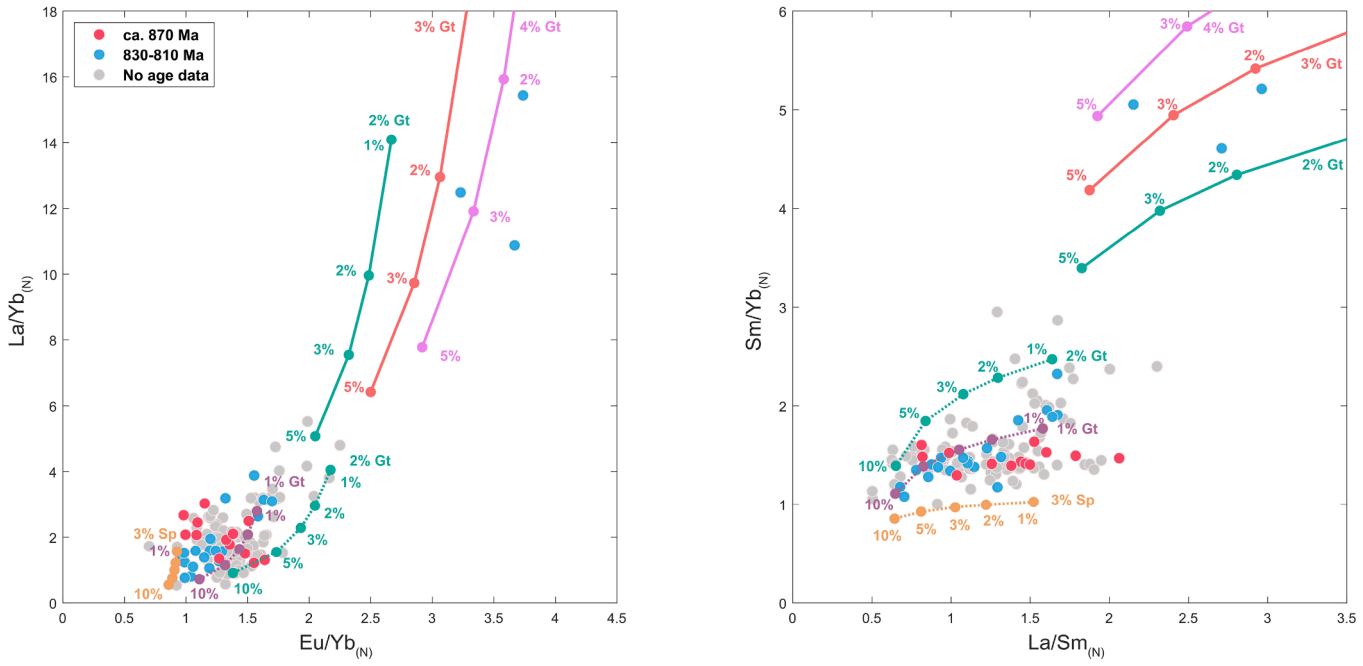

Fig. 11. Geochemical diagrams for the investigated mafic rocks. Plots of (A) $Eu/Yb_{(N)}$ vs. $La/Yb_{(N)}$ and (B) $La/Sm_{(N)}$ vs. $Sm/Yb_{(N)}$ for mafic rocks from the Dahongshan area. The melt curves are calculated based on the fractional melting model (after Lee et al., 2012) and circle marks along the curves represent the degree of partial melting. The dotted curves represent the melting of enriched DMM sources (Workman and Hart, 2005). The solid curves represent the melting of garnet-bearing lherzolite mantle sources (Jourdan et al., 2007). The Chondrite-normalized data are after Sun and McDonough (1989). Partition coefficients and modal proportions for spinel peridotite, garnet peridotite and garnet-bearing lherzolite are taken from Mckenzie and O'Nions (1991) and Jourdan et al. (2007). Data sources are the same as those in Fig. 5.

gabbroic suite and associated dioritic plutons in the northern Yangtze Block (Wu et al., 2016). The coeval ca. 820–800 Ma Huangling mafic to felsic intrusions were suggested to be unrelated to subduction of oceanic crust but linked to lithospheric extension (Zhang et al., 2008, 2009). As discussed above, the within-plate extension-related magmatism in the northern Yangtze Block was developed since ca. 830–820 Ma, which is roughly coincident with the onset of rifting in the eastern part of the Yangtze Block.

5.3. *Nature of magma source for the felsic rocks*

The behavior of zircon during magma generation and evolution is of major concern to geochemists due to its character of ubiquitousness and refractoriness (Schmitt, 2011; Keller et al., 2017). Zircon Hf isotopes can be used to distinguish magma sources of juvenile crust versus old crustal materials (Belousova et al., 2010; Dhuime et al., 2012). However, they cannot discern surficial processes that the source may have been modified previously, as the Hf isotopic system is insensitive to the hydrothermal alteration or weathering (Griffin et al., 2000). In contrast, stable isotopic system such as oxygen isotopes is useful in tracing the recycling of supracrustal rocks (Hawkesworth and Kemp, 2006; Roberts and Spencer, 2015). Zircon in equilibrium pristine mantle-derived melts have an average $\delta^{18}O$ values of 5.3 ± 0.6 ‰ (Valley, 2003), and deviations over the range can be attributed to incorporation of ^{18}O-enriched supracrustal component and below the range commonly explained by ^{18}O-depleted high-temperature hydrothermally altered component in the magma source. Therefore, zircon Hf-O isotopes jointly characterize relative contributions from mantle, crustal and sedimentary materials (Kemp et al., 2007).

As discussed above, the Dahongshan igneous suites can be divided into two stages. The Hf isotopic evolution pattern of the 970–840 Ma igneous rocks indicates a similar juvenile crustal source with a slight trend to relatively more evolved compositions since ca. 870 Ma (Fig. 9A), which suggests a transition from oceanic-arc to continental-arc subduction as proposed by Huang et al. (2021) based on detrital zircon studies. The gradually increasing zircon $\delta^{18}O$ values from 5.59–6.23 ‰ to 6.6–6.89 ‰ with time observed in ca. 970–840 Ma igneous rocks indicate the increased involvement of some ^{18}O-enriched crustal protoliths in their magma source (Fig. 9B), consistent with the expected more incorporation of continental components in a continental arc setting. In comparison, ca. 830–790 Ma igneous rocks display broad Hf isotopic distribution with both depleted mantle-like isotopic compositions and isotopically evolved pre-existing crust-like compositions, indicating multiple magma sources for their origins. The mantle-like $\delta^{18}O$ values of zircon from ca. 830–790 Ma igneous rocks indicate that minor or absent interaction of magmas with supracrustal materials. It is noted that the ca. 830 Ma rhyolites show $\delta^{18}O$ values in zircon lower than the mantle value, which is a feature of magmas experienced high-temperature hydrothermal alteration in an extensional setting. The rhyolites may also represent the oldest Neoproterozoic low-$\delta^{18}O$ igneous rocks exposed in northern Yangtze Block so far. They are consistent with the ca. 830 Ma ignimbrite with low-$\delta^{18}O$ (average 4.16 ‰) in the Jiangshan area, eastern part of the Jiangnan Orogen (Zhang et al., 2020), implying that low-$\delta^{18}O$ magmatism has developed in the two regions at least at ca. 830 Ma.

To estimate relative contributions of old crustal and juvenile components to produce the Hf-O isotopic compositions observed in the Dahongshan igneous suites, a simple binary mixing model is proposed here (Fig. 10). The crustal end-member could be Archean basements like the ancient rocks in the Kongling complex, but considering the systematics of such isotopic data and the expected less incorporation of old crust, the Neoproterozoic mature continental crust (folded metasedimentary sequences) of Wang et al. (2013) is adopted as the crustal end-member. The mantle end-member corresponds to Neoproterozoic juvenile crustal materials (Lu et al., 2020). As shown in the Fig. 10, except for the low-$\delta^{18}O$ rhyolites, the Dahongshan igneous suites generally show juvenile crust-like isotopic signature, close to the mantle end-member. The proportion of the incorporated mature crustal component in the source of Dahongshan magmas varies from 10–20 % for the ca. 970–840 Ma felsic rocks, and decreases to 0–10 % for the ca. 830–790 Ma rocks.

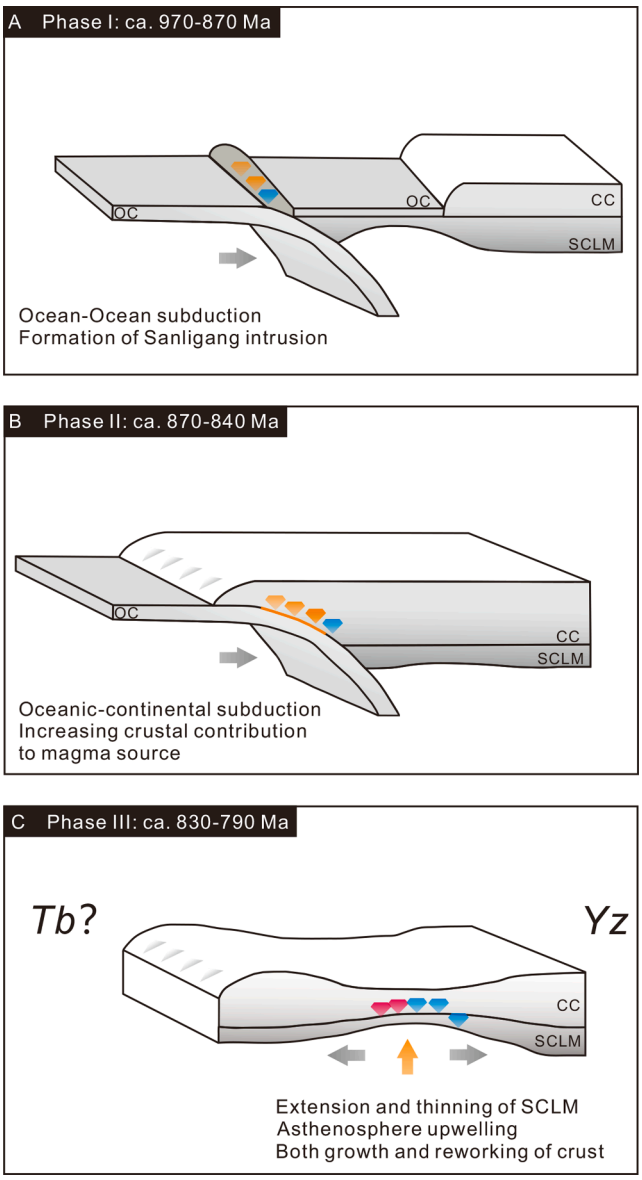

Fig. 12. A simplified three-stage tectonic evolution cartoon model of the Neoproterozoic tectono-magmatic activity in the Dahongshan area. Phase I: oceanic plate subduction with the formation of Sanligang intrusion. Phase II: oceanic-continental subduction, accretion and results in the development of extensive *retro*-arc fold, -thrust belts, accretionary complexes and arc-related igneous suites. The contribution of crustal material is increasing during this stage. Phase III: within-plate extension and thinning of sub-continental lithospheric mantle (SCLM), accompanied by asthenosphere upwelling and advective heat and formation of MORB- and OIB-like mafic suites and A_2-type felsic volcanic rocks. Tb: Tongbai Block; Yz: Yangtze Block.

It' noteworthy that some ca. 830–790 Ma felsic rocks with negative $\varepsilon_{Hf}(t)$ values are not shown in the Fig. 10 due to lack of O isotopic data. And the majority of ca. 970–840 Ma felsic rocks with 10–20 % ancient crust are indicative of continent arc-related rocks that formed between ca. 870–840 Ma, whereas ca. 970–870 Ma felsic rocks exhibit minor involvement of ancient crust as shown in Fig. 9, indicating reworking or the existence of juvenile crust.

5.4. Mantle source of the mafic rocks and tectonic model

Understanding the source characters of mafic rocks will provide important implications for tectonic evolution. REE can offer a unique insight into the mantle melting conditions based on their different partition behaviors in the spinel and garnet stability fields, which characterize the mantle aluminous phases (Wang et al., 2011; Condamine et al., 2022). To quantify a more realistic REE behavior during mantle melting, we applied fractional melting model for the depleted MORB mantle (DMM) peridotite [0.253 ppm La, 0.273 ppm Sm, 0.108 ppm Eu and 0.382 ppm Yb (Workman and Hart, 2005)] and garnet-bearing lherzolite [1.35 ppm La, 0.62 ppm Sm, 0.19 ppm Eu and 0.45 ppm Yb (Jourdan et al., 2007)] to generate a series of instantaneous fractional melts, which are then pooled following Lee et al. (2012). The REE contents and ratios in the aggregated melt are representative of the actual melt composition. The Dahongshan mafic rocks generally have low $La/Yb_{(N)}$ ratios (0.53–15.43), $Eu/Yb_{(N)}$ ratios (0.70–3.74), $La/Sm_{(N)}$ ratios (0.50–2.96) and $Sm/Yb_{(N)}$ ratios (1.00–5.21) as shown in Fig. 11, suggesting most of mafic rocks are formed as a result of low-degree (mostly < 5 %) partial melting of mantle peridotite. In the diagrams of $Eu/Yb_{(N)}$ vs. $La/Yb_{(N)}$ and $La/Sm_{(N)}$ vs. $Sm/Yb_{(N)}$, the majority of the samples can be modeled by 1–10 % melting of DMM between 3 % spinel and 2 % garnet, except three 830–810 Ma samples plot away from others and fall onto the garnet-bearing lherzolite (2–4 % garnet), which were suggested to be oceanic island basalts by Chen et al. (2017). The mantle source inclined to DMM (from 3 % spinel to 2 % garnet) indicates relative shallow melting depths for most Dahongshan Neoproterozoic mafic rocks, and a few 830–810 Ma mafic rocks may have been formed in a relatively deep level within garnet stability field. In addition, it is noted that the negative anomalies of Nb are more significant in the ca. 870 Ma mafic rocks than the ca. 830–810 mafic rocks (Fig. 6H, J), implying mantle metasomatism that possibly resulted from fluids released from the subducted slab. According to the geochemical and isotopic compositions and melting model, The formation of ca. 870 Ma arc-related mafic rocks in the Dahongshan area was probably associated with partial melting of the mantle wedge, whereas the emergence of ca. 830–810 Ma MORB- and OIB-like mafic rocks is thought to have resulted from the different degrees of partial melting of upwelling asthenosphere.

Combined with zircon Hf-O isotopic studies of the Neoproterozoic felsic rocks and the Hf isotopes in detrital zircon in the sediments in the Dahongshan area (Xu et al., 2016; Huang et al., 2021), the secular arc-related magmatism in the area appears to have undergone a tectonic transition from oceanic arc (depleted Hf isotopes and mantle-like oxygen isotopes) to continental arc (gradually increased $\delta^{18}O$ and arc-like geochemical affinity) and within-plate extension (co-occurrence of the MORB- and less OIB-like mafic suites and A_2-type felsic volcanic rocks) (Fig. 12). The development of *retro*-arc fold-and-thrust belts and extension-related igneous suites further highlights the transition of the tectonic regime in the Dahongshan area (Deng et al., 2013; Hu et al., 2015b; Yang et al., 2018; Liu and Zhao, 2019). The amalgamation in northern Yangtze Block may have displayed a "soft collision" feature at 840–830 Ma without exposure of *syn*-collisional assemblages and high-grade metamorphic rocks (Zhao, 2015), which resembles the collisional assembly between the Yangtze Block and Cathaysia Block along the Jiangnan Orogen. It is generally accepted that the Yangtze Block played a significant role in the reconstruction of the Rodinia supercontinent (Li et al., 2008; Cawood et al., 2016; Zhao et al., 2018b), but its position is controversial. In our opinion, the long-term subduction (at least from ca. 970 Ma to ca. 840 Ma) on the northern, southeastern and western margins of the Yangtze Block, the asynchronous igneous impulse and heterogeneous characters of the igneous activities (Huang et al., 2021) all indicate an external rather than an internal position of the block within the assembled Rodinia supercontinent.

6. Conclusions

The early to mid-Neoproterozoic mafic-felsic magmatism that occurred in the Dahongshan area serves as a significant record of enduring tectono-magmatic history along the northern margin of the Yangtze Block. In this study, we have produced and compiled a

geochemical data in the Dahongshan area including whole-rock compositions and zircon U-Pb-Hf-O isotopes. The Dahongshan igneous suites were emplaced at ca. 970–790 Ma, which recorded a continuous ca. 180 Myr-long magmatism, extending the time period of magmatic activity of the northern Yangtze Block. Geochemical analysis of the major and trace elements reveals that the igneous suites can be divided into two age groups. The older ca. 970–840 Ma intermediate-felsic rocks and mafic rocks both have a subduction-related tectonic setting. Positive zircon Hf and slightly high O isotope indicate a juvenile source with minor supracrustal incorporation. In comparison, the younger ca. 830–790 Ma mafic and felsic rocks formed in an extensional setting. The broad Hf isotopic distribution and mantle-like O isotopes indicate multiple magma sources for their origins and occurrence of high-temperature hydrothermal alteration. The Neoproterozoic magmatism on the northern margin of the Yangtze Block reflects a remarkable tectonic transition from subduction-accretion in ca. 970–840 Ma, accompanied by significant crustal growth, to within-plate extension at ca. 830–790 Ma with mainly reworking of juvenile and ancient crust.

CRediT authorship contribution statement

Yu Huang: Conceptualization, Methodology, Validation, Formal analysis, Investigation, Data curation, Writing – original draft, Visualization. **Xiao-Lei Wang:** Validation, Resources, Writing – review & editing, Supervision. **Jun-Yong Li:** Validation, Investigation. **Ru-Cao Li:** Investigation. **De-Hong Du:** Investigation. **Chang-Hong Jiang:** Investigation. **Lin-Sen Li:** Investigation. **Ning Ding:** Investigation.

Declaration of Competing Interest

The authors declare the following financial interests/personal relationships which may be considered as potential competing interests: Xiaolei Wang reports financial support was provided by Nanjing University. Xiaolei Wang reports a relationship with Nanjing University that includes: employment. There is no relationship or activity that may be interpreted as a conflict of interest by the reader.

Data availability

The data have been shared as the supplementary files.

Acknowledgements:

This work was financially supported by the National Natural Science Foundation of China (42025202), and the Fundamental Research Funds for the Central Universities of Ministry of Education (0206-14380176). The manuscript benefits from the constructive and thoughtful comments raised by Prof. Jinlong Yao and an anonymous reviewer. We thank Ru-Cao Li, Jun-Yong Li, De-Hong Du, Lin-Sen Li, Ning Ding for field work, Bing Wu for LA-ICP-MS zircon U-Pb dating, Chun Yang, Yue Guan and Lan-Lan Tian for SIMS zircon dating, and Dr. Tao Yang for LA-MC-ICP-MS zircon Hf isotope analysis.

Appendix A. Supplementary material

Supplementary data to this article can be found online at https://doi.org/10.1016/j.precamres.2023.107133.

References

Belousova, E.A., Kostitsyn, Y.A., Griffin, W.L., Begg, G.C., O'Reilly, S.Y., Pearson, N.J., 2010. The growth of the continental crust: Constraints from zircon Hf-isotope data. Lithos 119, 457–466.
Black, L.P., Gulson, B.L., 1978. The age of the mud tank carbonatite, strangways range, northern territory. BMR J. Aust. Geol. Geophys. 3 (3), 227–232.
Bonin, B., 2007. A-type granites and related rocks: Evolution of a concept, problems and prospects. Lithos 97, 1–29.
Bouvier, A., Vervoort, J.D., Patchett, P.J., 2008. The Lu–Hf and Sm–Nd isotopic composition of CHUR: Constraints from unequilibrated chondrites and implications for the bulk composition of terrestrial planets. Earth Planet. Sci. Lett. 273, 48–57.
Cawood, P.A., Strachan, R.A., Pisarevsky, S.A., Gladkochub, D.P., Murphy, J.B., 2016. Linking collisional and accretionary orogens during Rodinia assembly and breakup: Implications for models of supercontinent cycles. Earth Planet. Sci. Lett. 449, 118–126.
Cawood, P.A., Zhao, G., Yao, J., Wang, W., Xu, Y., Wang, Y., 2018. Reconstructing South China in Phanerozoic and Precambrian supercontinents. Earth Sci. Rev. 186, 173–194.
Cawood, P.A., Wang, W., Zhao, T., Xu, Y., Mulder, J.A., Pisarevsky, S.A., Zhang, L., Gan, C., He, H., Liu, H., Qi, L., Wang, Y., Yao, J., Zhao, G., Zhou, M.-F., Zi, J.-W., 2020. Deconstructing South China and consequences for reconstructing Nuna and Rodinia. Earth Sci. Rev. 204, 103169.
Chen, K., Gao, S., Wu, Y., Guo, J., Hu, Z., Liu, Y., Zong, K., Liang, Z., Geng, X., 2013. 2.6–2.7Ga crustal growth in Yangtze craton, South China. Precambr. Res. 224, 472–490.
Chen, C., Mao, X.-W., Hu, Z.-X., Yang, J.-X., Yang, C., Kong, L.-Y., Meng, Z., 2017. Discovery of~ 817 Ma oceanic island basalts in the Dahongshan region, northern Hubei Province and its significance. Geol. Sci. Technol. Inf. 36 (6), 22–31 (in Chinese with English abstract).
Condamine, P., Couzinié, S., Fabbrizio, A., Devidal, J.-L., Médard, E., 2022. Trace element partitioning during incipient melting of phlogopite-peridotite in the spinel and garnet stability fields. Geochim. Cosmochim. Acta 327, 53–78.
Condie, K.C., Aster, R.C., 2010. Episodic zircon age spectra of orogenic granitoids: The supercontinent connection and continental growth. Precambr. Res. 10.
Cui, X., 2020. Paleoproterozoic tectonic evolution of the Yangtze Block_New evidence from ca. 2.36 to 2.22 Ga magmatism and 1.96 Ga metamorphism in the Cuoke complex, SW China. Precambr. Res. 20.
Cui, X., Wang, J., Wang, X.-C., Wilde, S.A., Ren, G., Li, S., Deng, Q., Ren, F., Liu, J., 2021. Early crustal evolution of the Yangtze Block: Constraints from zircon U-Pb-Hf isotope systematics of 3.1–1.9 Ga granitoids in the Cuoke Complex, SW China. Precambr. Res. 357, 106155.
Deng, Q., Wang, J., Wang, Z.-J., Wang, X.-C., Qiu, Y.-S., Yang, Q.-X., Du, Q.-D., Cui, X.-Z., Zhou, X.-L., 2013. Continental flood basalts of the Huashan Group, northern margin of the Yangtze block – implications for the breakup of Rodinia. Int. Geol. Rev. 55, 1865–1884.
Deng, Q., 2013. Middle Neoproterozoic stratigraphic framework and basin evolution in the norther margin of Yangtze Block. (Doctoral Thesis). Chinese Academy of Geological Sciences (in Chinese with English abstract).
Dhuime, B., Hawkesworth, C.J., Cawood, P.A., Storey, C.D., 2012. A Change in the Geodynamics of Continental Growth 3 Billion Years Ago. Science 335, 1334–1336.
Dong, Y., 2004. Geochemistry of the subduction-related magmatic rocks in the Dahong Mountains, northern Hubei Province —Constraint on the existence and subduction of the eastern Mianlve oceanic basin. Sci. China Ser. D: Earth Sci. 47, 366.
Dong, Y.-P., Zhang, G.-W., Lai, S.-C., Zhou, D.-W., Zhu, B.-Q., 1999. Definition of the Huashan ophiolite complex in the Suizhou area and its tectonic significance. Sci. China (Ser. D) 29 (3), 222–231 (in Chinese with English abstract).
Eby, G.N., 1992. Chemical subdivision of the A-type granitoids: Petrogenetic and tectonic implications. Geology 20, 641.
Evans, D.A.D., 2013. Reconstructing pre-Pangean supercontinents. Geol. Soc. Am. Bull. 125, 1735–1751.
Gao, S., Yang, J., Zhou, L., Li, M., Hu, Z., Guo, J., Yuan, H., Gong, H., Xiao, G., Wei, J., 2011. Age and growth of the Archean Kongling terrain, South China, with emphasis on 3.3 ga granitoid gneisses. Am. J. Sci. 311, 153–182.
Griffin, W.L., Powell, W.J., Pearson, N.J., O'Reilly, S.Y., 2008. GLITTER: data reduction software for laser ablation ICP-MS. In: Sylvester, P. (Ed.), Laser Ablation-ICP-MS in the Earth Sciences, Mineralogical Association of Canada Short Course Series, 40, pp. 204–207 (Appendix 2).
Griffin, W.L., Pearson, N.J., Belousova, E., Jackson, S.E., van Achterbergh, E., O'Reilly, S. Y., Shee, S.R., 2000. The Hf isotope composition of cratonic mantle: LAM-MC-ICPMS analysis of zircon megacrysts in kimberlites. Geochim. Cosmochim. Acta 64, 133–147.
Hawkesworth, C.J., Dhuime, B., Pietranik, A.B., Cawood, P.A., Kemp, A.I.S., Storey, C.D., 2010. The generation and evolution of the continental crust. J. Geol. Soc. London 167, 229–248.
Hawkesworth, C.J., Cawood, P.A., Dhuime, B., Kemp, T.I.S., 2017. Earth's Continental Lithosphere Through Time. Annu. Rev. Earth Planet. Sci. 45, 169–198.
Hawkesworth, C.J., Cawood, P.A., Dhuime, B., 2020. The Evolution of the Continental Crust and the Onset of Plate Tectonics. Front. Earth Sci. 8, 326.
Hawkesworth, C.J., Kemp, A.I.S., 2006. Using hafnium and oxygen isotopes in zircons to unravel the record of crustal evolution. Chem. Geol. 226, 144–162.
Hou, G., Santosh, M., Qian, X., Lister, G.S., Li, J., 2008. Configuration of the Late Paleoproterozoic supercontinent Columbia: Insights from radiating mafic dyke swarms. Gondw. Res. 14, 395–409.
Hu, Z.-X., Chen, C., Mao, X.-W., Yang, Q.-X., Deng, Q.-Z., Kong, L.-Y., Yang, C., 2015a. Documentation of Jingningian island-arc volcanic rocks and accretionary complexes in the Dahongshan region, northern Hubei and its tectonic significance. Resour. Environ. Eng. 29 (6), 757–766 (in Chinese with English abstract).
Hu, Z.-X., Mao, X.-W., Tian, W.-X., Li, X.-W., 2015b. Discovery of the Jinningian Orogenic Belt on the northern margin of Yangtze Craton in Mountain Dahong. Geol. Surv. China 2 (2), 33–39 (in Chinese with English abstract).
Hu, Z.-X., Chen, C., Mao, X.-W., Yang, Q.-X., Deng, Q.-Z., Kong, L.-Y., Yang, C., 2017. The Qingbaikouan Tumen Formation-complex Island arc volcanic-clastic rocks on the northern margin of Yangtze Block and its significance. J. Stratigr. 41 (3), 304–317 (in Chinese with English abstract).

Huang, D., Wang, X., Xia, X., Wan, Y., Zhang, F., Li, J., Du, D., 2019. Neoproterozoic Low-δ 18 O Zircons Revisited: Implications for Rodinia Configuration. Geophys. Res. Lett. 46, 678–688.
Huang, Y., Wang, X.-L., Li, J.-Y., Wang, D., Jiang, C.-H., Li, L.-S., 2021. Early Neoproterozoic tectonic evolution of northern Yangtze Block: Insights from sedimentary sequences from the Dahongshan area. Precambr. Res. 365, 106382.
Iles, K.A., Hergt, J.M., Sircombe, K.N., Woodhead, J.D., Bodorkos, S., Williams, I.S., 2015. Portrait of a reference material: Zircon production in the Middledale Gabbroic Diorite, Australia, and its implications for the TEMORA standard. Chem. Geol. 402, 140–152.
Irvine, T.N., Baragar, W.R.A., 1971. A Guide to the Chemical Classification of the Common Volcanic Rocks. Can. J. Earth Sci. 8, 523–548.
Jackson, S.E., Pearson, N.J., Griffin, W.L., Belousova, E.A., 2004. The application of laser ablation-inductively coupled plasma-mass spectrometry to in situ U-Pb zircon geochronology. Chem. Geol. 211, 47–69.
Jourdan, F., Bertrand, H., Schärer, U., Blichert-Toft, J., Féraud, G., Kampunzu, A.B., 2007. Major and Trace Element and Sr, Nd, Hf, and Pb Isotope Compositions of the Karoo Large Igneous Province, Botswana–Zimbabwe: Lithosphere vs Mantle Plume Contribution. J. Petrol. 48, 1043–1077.
Keller, C.B., Boehnke, P., Schoene, B., 2017. Temporal variation in relative zircon abundance throughout Earth history. Geochem. Perspect. Lett. 179–189.
Kemp, A.I.S., Hawkesworth, C.J., Foster, G.L., Paterson, B.A., Woodhead, J.D., Hergt, J. M., Gray, C.M., Whitehouse, M.J., 2007. Magmatic and Crustal Differentiation History of Granitic Rocks from Hf-O Isotopes in Zircon. Science 315, 980–983.
Le, W., Kusky, T.M., Wei, J., Jie, Y., Zuoxun, Z., 2021. Neoproterozoic tectonics of the Jiangnan orogen: The magmatic record of continental growth by arc and slab-failure magmatism from 1000 to 780 Ma. Precambr. Res. 362, 106319.
Lee, C.T.A., Luffi, P., Chin, E.J., Bouchet, R., Dasgupta, R., Morton, D.M., Roux, V.L., Yin, Q.-Z., Jin, D., 2012. Copper systematics in arc magmas and implications for crust-mantle differentiation. Science 336 (6077), 64–68.
Li, Z.X., Bogdanova, S.V., Collins, A.S., Davidson, A., De Waele, B., Ernst, R.E., Fitzsimons, I.C.W., Fuck, R.A., Gladkochub, D.P., Jacobs, J., Karlstrom, K.E., Lu, S., Natapov, L.M., Pease, V., Pisarevsky, S.A., Thrane, K., Vernikovsky, V., 2008. Assembly, configuration, and break-up history of Rodinia: A synthesis. Precambr. Res. 160, 179–210.
Li, K., Deng, Q., Hou, M., Wang, J., Yakymchuk, C., Cui, X., Ren, G., Wang, Z., 2020a. Geochronology and sedimentology of the Huashan Group in the northern Yangtze Block: implications for the initial breakup of the South China. Int. J. Earth Sci. 109, 2113–2131.
Li, K., Deng, Q., Wang, J., Hou, M., Yakymchuk, C., Cui, X., Ren, G., Wang, Z., Dai, J., Chen, B., 2020b. Detrital zircon in the Huashan Group, northern Yangtze Block: Implications for the nature of Neoproterozoic sedimentary basins and Precambrian crustal evolution. Geol. J. 55 (12), 8211–8224.
Li, L., Lin, S., Davis, D.W., Xiao, W., Xing, G., Yin, C., 2014. Geochronology and geochemistry of igneous rocks from the Kongling terrane: Implications for Mesoarchean to Paleoproterozoic crustal evolution of the Yangtze Block. Precambr. Res. 255, 30–47.
Li, X.-H., Liu, Y., Li, Q.-L., Guo, C.-H., Chamberlain, K.R., 2009. Precise determination of Phanerozoic zircon Pb/Pb age by multi-collector SIMS without external standardization. Geochem. Geophys. Geosyst. 10, Q04010.
Li, X.-H., Long, W.-G., Li, Q.-L., Liu, Y., Zheng, Y.-F., Yang, Y.-H., Chamberlain, K.R., Wan, D.-F., Guo, C.-H., Wang, X.-C., Tao, H., 2010. Penglai zircon megacrysts: a potential new working reference material for microbeam determination of Hf–O isotopes and U-Pb age. Geostand. Geoanal. Res. 34 (2), 117–134.
Li, X.-H., Tang, G.-Q., Gong, B., Yang, Y.-H., Hou, K.-J., Hu, Z.-C., Li, Q.-L., Liu, Y., Li, W.-X., 2013. Qinghu zircon: A working reference for microbeam analysis of U-Pb age and Hf and O isotopes. Chin. Sci. Bull. 58, 4647–4654.
Li, H.-K., Tian, H., Zhou, H.-Y., Zhang, J., Liu, H., Geng, J.-Z., Ye, L.-J., Xiang, Z.-Q., Qu, L.-S., 2016. Correlation between the Dagushi Group in the Dahongshan area and the Shennongjia Group in the Shennongjia Area on the northern margin of the Yangtze Craton: Constraints from zircon U-Pb ages and Lu-Hf isotopic systematics. Earth Sci. Front. 23 (6), 186–201 (in Chinese with English abstract).
Li, J.-Y., Wang, X.-L., Gu, Z.-D., 2018a. Petrogenesis of the Jiaoziding granitoids and associated basaltic porphyries: Implications for extensive early Neoproterozoic arc magmatism in western Yangtze Block. Lithos 296–299, 547–562.
Li, J.-Y., Wang, X.-L., Gu, Z.-D., 2018b. Early Neoproterozoic arc magmatism of the Tongmuliang Group on the northwestern margin of the Yangtze Block: Implications for Rodinia assembly. Precambr. Res. 309, 181–197.
Li, J.-Y., Wang, X.-L., Wang, D., Du, D.-H., Yu, J.-H., Gu, Z.-D., Huang, Y., Li, L.-S., 2021. Pre-Neoproterozoic continental growth of the Yangtze Block: From continental rifting to subduction–accretion. Precambr. Res. 355, 106081.
Li, L.-S., Wang, X.L., Yakymchuk, C., Schorn, S., Yu, J.-H., Wang, D., Li, J.Y., Du, D.H., Huang, Y., 2022. A refined study of Paleoproterozoic high-pressure granulite-facies metamorphism in the Kongling Complex of northern Yangtze Block. Precambr. Res. 378, 106741.
Liao, M.-F., Xie, Y.-B., Li, L.-J., Yang, J.-X., Mao, X.-W., Deng, Q.-Z., Kong, L.-Y., Li, Q.-W., Chen, C., 2016. Discussion about genesis and formation age of Sanligang pluton in the Dahongshan Region. Hubei. Resour. Environ. Eng. 30 (02), 143–150+158 (in Chinese with English abstract).
Ling, W.-L., Gao, S., Zhang, B.-R., Zhou, L., Xu, Q.-D., 2000. Late Paleoproterozoic tectonic-thermal events of the Yangtze continental nucleus and the Yangtze craton's evolution. Chin. Sci. Bull. 45 (21), 2343–2348 (in Chinese with English abstract).
Liu, Y., Mitchell, R.N., Li, Z.-X., Kirscher, U., Pisarevsky, S.A., Wang, C., 2021. Archean geodynamics: Ephemeral supercontinents or long-lived supercratons. Geology 49, 794–798.
Liu, Y., Xu, Y., Ali, P., Yang, K.-G., Zhou, Q., Wu, P., Yang, Z.-N., 2022. 840–820 Ma Dahongshan bimodal volcanic rocks: new constraints on the Neoproterozoic arc–back-arc basin system along the northern margin of the Yangtze Block. Int. Geol. Rev. 1–32.
Liu, S.-D., Zeng, Z.-X., Guo, R.-L., Zhang, X., 2020. Huashan Group in northern margin of Yangtze block: a suite of backarc-basin volcanic-sedimentary strata but not ophiolite mélange. Earth Sci. 46 (8), 2751–2767 (in Chinese with English abstract).
Liu, H., Zhao, J.-H., 2019. Slab breakoff beneath the northern Yangtze Block: Implications from the Neoproterozoic Dahongshan mafic intrusions. Lithos 342–343, 263–275.
Loiselle, M.C., Wones, D.R., 1979. Characteristics of anorogenic granites. Geol. Soc. Am. Abstr. Programs 11, 468.
Lu, K., Li, X.-H., Zhou, J.-L., Peng, S.-B., Deng, H., Guo, S., Yang, C., Wu, L.-G., 2020. Early Neoproterozoic assembly of the Yangtze Block decoded from metasedimentary rocks of the Miaowan Complex. Precambr. Res. 346, 105787.
Ludwig, K.R., 2001. Isoplot/Ex(rev). 2.49: a geochronological toolkit for Microsoft Excel. Berkeley Geochronological Center. Special Publications 1a, 1–58.
Ludwig, R., 2003. Electrochemically induced reactions in soils: a new approach to the in-situ remediation of contaminated soils? Part 1: The microconductor principle. Electrochim. Acta 47 (9), 1395–1403.
Mckenzie, D., O'Nions, R.K., 1991. Partial Melt Distributions from Inversion of Rare Earth Element Concentrations. J. Petrol. 32, 1021–1091.
Meert, J.G., 2012. What's in a name? The Columbia (Paleopangaea/Nuna) supercontinent. Gondw. Res. 21, 987–993.
Merdith, A.S., Collins, A.S., Williams, S.E., Pisarevsky, S., Foden, J.D., Archibald, D.B., Blades, M.L., Alessio, B.L., Armistead, S., Plavsa, D., Clark, C., Müller, R.D., 2017. A full-plate global reconstruction of the Neoproterozoic. Gondw. Res. 50, 84–134.
Miller, C.F., McDowell, S.M., Mapes, R.W., 2003. Hot and cold granites? Implications of zircon saturation temperatures and preservation of inheritance. Geology 31, 529.
Mitchell, R.N., Zhang, N., Salminen, J., Liu, Y., Spencer, C.J., Steinberger, B., Murphy, J. B., Li, Z.-X., 2021. The supercontinent cycle. Nat. Rev. Earth Environ. 2, 358–374.
Mulder, J.A., Nebel, O., Gardiner, N.J., Cawood, P.A., Wainwright, A.N., Ivanic, T.J., 2021. Crustal rejuvenation stabilised Earth's first cratons. Nat. Commun. 12, 3535.
Nance, R.D., Murphy, J.B., Santosh, M., 2014. The supercontinent cycle: A retrospective essay. Gondw. Res. 25, 4–29.
Nasdala, L., Hofmeister, W., Norberg, N., Martinson, J.M., Corfu, F., Dörr, W., Kamo, S.L., Kennedy, A.K., Kronz, A., Reiners, P.W., Frei, D., Kosler, J., Wan, Y., Götze, J., Häger, T., Kröner, A., Valley, J.W., 2008. Zircon M257 - a Homogeneous Natural Reference Material for the Ion Microprobe U-Pb Analysis of Zircon. Geostand. Geoanal. Res. 32, 247–265.
Pearce, J.A., 1982. Trace element characteristics of lavas from destructive plate boundaries. In: Thorpe, R.S. (Ed.), Orogenic Andesites. Wiley, Chichester, U.K., pp. 528–548
Pearce, J.A., 2014. Immobile element fingerprinting of ophiolites. Elements 10, 101–108.
Pearce, J.A., Harris, N.B.W., Tindle, A.G., 1984. Trace element discrimination diagrams for the tectonic interpretation of granitic rocks. J. Petrol. 25, 956–983.
Reddy, S.M., Evans, D.A.D., 2009. Palaeoproterozoic supercontinents and global evolution: correlations from core to atmosphere. Geol. Soc. Lond. Spec. Publ. 323 (1), 1–26.
Roberts, N.M.W., 2012. Increased loss of continental crust during supercontinent amalgamation. Gondw. Res. 21 (4), 994–1000.
Roberts, N.M.W., 2013. The boring billion? – Lid tectonics, continental growth and environmental change associated with the Columbia supercontinent. Geosci. Front. 4, 681–691.
Roberts, N.M.W., Spencer, C.J., 2015. The zircon archive of continent formation through time. Special Publications 389, 197–225.
Scherer, E., Münker, C., Mezger, K., 2001. Calibration of the Lutetium-Hafnium Clock. Science 293, 683–687.
Schmitt, A.K., 2011. Uranium Series Accessory Crystal Dating of Magmatic Processes. Annu. Rev. Earth Planet. Sci. 39, 321–349.
Shi, Y.-R., Zhang, Z.-Q., Liu, D.-Y., Tang, S.-H., Wang, J.-H., 2003. A study on Sm-Nd and Rb-Sr isotopic chronology of the Huashan ophiolitic Melange in the Suizhou Area, Hubei Province. Geol. Rev. 49 (4), 367–373 (in Chinese with English abstract).
Shi, Y.-R., Zhang, Z.-Q., Liu, D.-Y., Tang, S.-H., Wang, J.-H., Liu, T., 2005. Rb-Sr Isotope Dating of Gabbro from Yangjiapeng Area in Suizhou, Hubei Province. Acta Geosci. Sin. 6, 521–524 (in Chinese with English abstract).
Shi, Y.-R., Li, D.-Y., Zhang, Z.-Q., Miao, L.-C., Zhang, F.-Q., Xue, H.-M., 2007. SHRIMP Zircon U-Pb Dating of Gabbro and Granite from the Huashan Ophiolite, Qinling Orogenic Belt, China: Neoproterozoic Suture on the Northern Margin of the Yangtze Craton. Acta Geol. Sin. – Engl. Ed. 81, 239–243.
Shu, L., Wang, J., Yao, J., 2019. Tectonic evolution of the eastern Jiangnan region, South China: New findings and implications on the assembly of the Rodinia supercontinent. Precambr. Res. 322, 42–65.
Sláma, J., Košler, J., Condon, D.J., et al., 2008. Plešovice zircon — a new natural reference material for U-Pb and Hf isotopic microanalysis. Chem. Geol. 249 (1–2), 1–353.
Sun, S.-S., McDonough, W.F., 1989. Chemical and isotopic systematics of oceanic basalts: implications for mantle composition and processes. Spec. Publ. 42, 313–345.
Sun, Z.-M., Wang, X.-L., Zhang, F.-F., Xie, H.-Q., Zhao, K., Li, J.-Y., 2020. Diversity of felsic rocks in oceanic crust: Implications from the Neoproterozoic plagiogranites within the Northeast Jiangxi ophiolite, southern China. J. Geophys. Res.: Solid Earth 125, e2019JB017414.
Tian, H., Li, H.-K., Zhou, H.-Y., Zhang, J., Zhang, K., Geng, J.-Z., Xiang, Z.-Q., Qu, L.-S., 2017. Depositional age of the Huashan Group on the northern margin of the Yangtze plate and its constraints on breakup of the Rodinia supercontinent. Acta Geol. Sin. 91 (11), 2387–2408 (in Chinese with English abstract).

Valley, J.W., 2003. Oxygen isotope in zircon. In: Hanchar, J.M., Hoskin, P.W.O. (Eds.), Reviews in Mineralogy and Geochemistry: Zircon. Mineralogical Society of America, Washington, pp. 343–380.
Valley, J.W., Kinny, P.D., Schulze, D.J., Spicuzza, M.J., 1998. Zircon megacrysts from kimberlite: oxygen isotope variability among mantle melts. Contrib. Miner. Petrol. 133, 1–11.
Wang, C., Mitchell, R.N., Murphy, J.B., Peng, P., Spencer, C.J., 2020. The role of megacontinents in the supercontinent cycle. Geology 49 (4), 402–406.
Wang, X.-L., Jiang, S.-Y., Dai, B.-Z., Griffin, W.L., Dai, M.-N., Yang, Y.-H., 2011. Age, geochemistry and tectonic setting of the Neoproterozoic (ca 830 Ma) gabbros on the southern margin of the North China Craton. Precambr. Res. 190, 35–47.
Wang, X., Lü, Q., Cao, D., Guo, W., Peng, R., 2021. Geochronology, geochemistry and zircon Hf-O isotopic composition of ore-bearing volcanic rocks at Dapingzhang VMS Cu-Zn deposit, SW China: Petrogenetic, metallogenic and tectonic implications. Ore Geol. Rev. 133, 104040.
Wang, X.L., Zhou, J.C., Griffin, W.L., Wang, R.C., Qiu, J.S., O'Reilly, S.Y., Xu, X.S., Liu, X. M., Zhang, G.L., 2007. Detrital zircon geochronology of Precambrian basement sequences in the Jiangnan orogen: dating the assembly of the Yangtze and Cathaysia blocks. Precambr. Res. 159, 117–131.
Wang, X.-L., Zhou, J.-C., Wan, Y.-S., Kitajima, K., Wang, D., Bonamici, C., Qiu, J.-S., Sun, T., 2013. Magmatic evolution and crustal recycling for Neoproterozoic strongly peraluminous granitoids from southern China: Hf and O isotopes in zircon. Earth Planet. Sci. Lett. 366, 71–82.
Wang, X.-L., Zhou, J.-C., Griffin, W.L., Zhao, G., Yu, J.-H., Qiu, J.-S., Zhang, Y.-J., Xing, G.-F., 2014. Geochemical zonation across a Neoproterozoic orogenic belt: Isotopic evidence from granitoids and metasedimentary rocks of the Jiangnan orogen, China. Precambr. Res. 242, 154–171.
Whalen, J.B., Currie, K.L., Chappell, B.W., 1987. A-type granites: geochemical characteristics, discrimination and petrogenesis. Contrib. Miner. Petrol. 95, 407–419.
Wiedenbeck, M., Alle, P., Corfu, F., Griffin, W.L., Meier, M., Oberli, F., Vonquadt, A., Roddick, J.C., Speigel, W., 1995. Three natural zircon standards for U-Th–Pb, Lu–Hf, trace-element and REE analyses. Geostandard Newsletter 19, 1–23.
Workman, R.K., Hart, S.R., 2005. Major and trace element composition of the depleted MORB mantle (DMM). Earth Planet. Sci. Lett. 231, 53–72.
Wu, H., Zhang, Y.-H., Ling, W.-L., Bai, X., Ma, Q., Berkana, W., Cheng, J.-P., Peng, L.-H., 2016. Recognition of mantle input and its tectonic implication for the nature of ~815 Ma magmatism in the Yangtze continental interior, South China. Precambr. Res. 279, 17–36.
Xie, J.-H., Hu, Z.-X., Mao, X.-W., Kong, L.-Y., Yang, Q.-X., Yang, C., Guo, P., 2019. The discrimination of Jinningian MORB-like basalt and intra- oceanic subduction in the Dahongshan area, Northern Hubei. Geol. China 46 (6), 1496–1511 (in Chinese with English abstract).
Xu, Y., Yang, K.-G., Polat, A., Yang, Z.-N., 2016. The ~860 Ma mafic dikes and granitoids from the northern margin of the Yangtze Block, China: A record of oceanic subduction in the early Neoproterozoic. Precambr. Res. 275, 310–331.
Yan, C., Shu, L., Faure, M., Chen, Y., Huang, R., 2019. Time constraints on the closure of the Paleo-South China Ocean and the Neoproterozoic assembly of the Yangtze and Cathaysia blocks: Insight from new detrital zircon analyses. Gondw. Res. 73, 175–189.
Yang, Z.-N., Yang, K.-G., Polat, A., Xu, Y., 2018. Early crustal evolution of the eastern Yangtze Block: Evidence from detrital zircon U-Pb ages and Hf isotopic composition of the Neoproterozoic Huashan Group in the Dahongshan area. Precambr. Res. 309, 248–270.
Yang, Z.-N., 2017. The Paleoproterozoic to Middle Neoproterozoic tectonic evolution of the Suizhou-Yingshan terrain and its surrounding area in the northern Yangtze Block. (Doctoral Thesis). China University of Geosciences, Wuhan (in Chinese with English abstract).
Yao, J., Cawood, P.A., Shu, L., Zhao, G., 2019. Jiangnan Orogen, South China: A ~970–820 Ma Rodinia margin accretionary belt. Earth Sci. Rev. 196, 102872.
Yin, C.-Q., Lin, S.-F., Davis, D.W., Zhao, G.-C., Xiao, W.-J., Li, L.-M., He, Y.-H., 2013. 2.1–1.85Ga tectonic events in the Yangtze Block, South China: Petrological and geochronological evidence from the Kongling Complex and implications for the reconstruction of supercontinent Columbia. Lithos 182–183, 200–210.
Zerkle, A.L., 2018. Biogeodynamics: bridging the gap between surface and deep Earth processes. Philos. Trans. R. Soc. A Math. Phys. Eng. Sci. 376 (2132), 20170401.
Zhang, H., Liu, Y., Ding, X., Gao, L., Yang, C., Zhang, J., Gong, C., Liu, H., 2020. Geochronology, geochemistry, whole rock Sr-Nd and zircon Hf-O isotopes of the early Neoproterozoic volcanic rocks in Jiangshan, eastern part of the Jiangnan Orogen: Constraints on petrogenesis and tectonic implications. Acta Geol. Sin. – Engl. Ed. 94 (4), 1117–1137.
Zhang, S.-B., Zheng, Y.-F., Wu, Y.-B., Zhao, Z.-F., Gao, S., Wu, F.-Y., 2006a. Zircon U-Pb age and Hf isotope evidence for 3.8 Ga crustal remnant and episodic reworking of Archean crust in South China. Earth Planet. Sci. Lett. 252, 56–71.
Zhang, S.-B., Zheng, Y.-F., Wu, Y.-B., Zhao, Z.-F., Gao, S., Wu, F.-Y., 2006b. Zircon isotope evidence for ≥3.5 Ga continental crust in the Yangtze craton of China. Precambr. Res. 146 (1–2), 16–34.
Zhang, S.-B., Zheng, Y.-F., Zhao, Z.-F., Wu, Y.-B., Yuan, H., Wu, F.-Y., 2008. Neoproterozoic anatexis of Archean lithosphere: Geochemical evidence from felsic to mafic intrusions at Xiaofeng in the Yangtze Gorge, South China. Precambr. Res. 163, 210–238.
Zhang, S.-B., Zheng, Y.-F., Zhao, Z.-F., Wu, Y.-B., Yuan, H., Wu, F.-Y., 2009. Origin of TTG-like rocks from anatexis of ancient lower crust: Geochemical evidence from Neoproterozoic granitoids in South China. Lithos 113, 347–368.
Zhao, G., 2015. Jiangnan Orogen in South China: Developing from divergent double subduction. Gondw. Res. 27, 1173–1180.
Zhao, G., Cawood, P.A., 2012. Precambrian geology of China. Precambr. Res. 222–223, 13–54.
Zhao, G., Cawood, P.A., Wilde, S.A., Sun, M., 2002. Review of global 2.1–1.8 Ga orogens: implications for a pre-Rodinia supercontinent. Earth Sci. Rev. 59, 125–162.
Zhao, J.-H., Li, Q.-W., Liu, H., Wang, W., 2018b. Neoproterozoic magmatism in the western and northern margins of the Yangtze Block (South China) controlled by slab subduction and subduction-transform-edge-propagator. Earth Sci. Rev. 187, 1–18.
Zhao, G., Sun, M., Wilde, S.A., Li, S., 2004. A Paleo-Mesoproterozoic supercontinent: assembly, growth and breakup. Earth Sci. Rev. 67, 91–123.
Zhao, G., Wang, Y., Huang, B., Dong, Y., Li, S., Zhang, G., Yu, S., 2018a. Geological reconstructions of the East Asian blocks: From the breakup of Rodinia to the assembly of Pangea. Earth Sci. Rev. 186, 262–286.
Zhao, J.-H., Zhou, M.-F., Zheng, J.-P., 2013a. Neoproterozoic high-K granites produced by melting of newly formed mafic crust in the Huangling region, South China. Precambr. Res. 233, 93–107.
Zhao, J.-H., Zhou, M.-F., Zheng, J.-P., Griffin, W.L., 2013b. Neoproterozoic tonalite and trondhjemite in the Huangling complex, South China: Crustal growth and reworking in a continental arc environment. Am. J. Sci. 313, 540–583.
Zheng, Y.-F., Gong, B., Zhao, Z.-F., Wu, Y.-B., Chen, F.-K., 2008. Zircon U-Pb age and O isotope evidence for Neoproterozoic low-^{18}O magmatism during supercontinental rifting in South China: Implications for the snowball earth event. Am. J. Sci. 308 (4), 484–516.
Zhou, Y., Zhong, H., Zhu, W.-G., Bai, Z.-J., Li, C., 2022. Neoproterozoic protracted arc basaltic magmatism in the southern margin of the Yangtze Block, south China: New constraints from mafic-ultramafic intrusive rocks. Precambr. Res. 368, 106482.
Zou, H., Li, Q.-L., Bagas, L., Wang, X.-C., Chen, A.-Q., Li, X.-H., 2021. A Neoproterozoic low- δ^{18}O magmatic ring around South China: Implications for configuration and breakup of Rodinia supercontinent. Earth Planet. Sci. Lett. 575, 117196.